THE GEOLOGIC RECORD OF PALEOSTORMS FROM LAKE AND WETLAND SEDIMENTS OF THE GREAT PLAINS

By

MARK MCCOLLUM

Bachelor of Science in Geology

Baylor University

Waco, Texas

2013

Submitted to the Faculty of the
Graduate College of the
Oklahoma State University
in partial fulfillment of
the requirements for
the Degree of
MASTER OF SCIENCE
May, 2015

THE GEOLOGIC RECORD OF PALEOSTORMS

FROM LAKE AND WETLAND SEDIMENTS OF THE

GREAT PLAINS

Thesis Approved:

Joseph Donoghue

Thesis Adviser

Mohamed Abdelsalam

Jeffrey Byrnes

ACKNOWLEDGEMENTS

I first would like to thank my adviser Dr. Joseph Donoghue for giving me the opportunity to conduct this study. Without his supervision this document would have not been possible. I would also like to thank my committee members Dr. Jeffrey Byrnes, Dr. Eliot Atekwana, and Dr. Mohamed Abdel Salam for their edits and wisdom which allowed for the completion of this document.

I would like to thank Dr. Art Lucas and all the assistance he gave us with the gamma ray spectrometer data collection process and analysis. I would also like to thank Michelle Lutiker, Hannah Sanders, and Grace Waresback for their assistance in helping to prepare samples and run them through the CILAS particle analyzer. I also thank Tyler McNabb for his assistance in core collection. I would also like to thank my girlfriend, Kate Taylor, for her constant support and help with sample preparation and data collection.

I would like to thank Cheyenne Bottoms Wildlife Refuge for allowing us to take multiple cores on their land and for their field support. I also thank the Corps of Engineers staff stationed at Canton Lake, OK, for allowing us to take cores in the lake.

This research was grant supported by the Geological Society of America and the Society for Sedimentary Geology.

Name: MARK MCCOLLUM

Date of Degree: MAY, 2015

Title of Study: THE GEOLOGIC RECORD OF PALEOSTORMS FROM LAKE AND WETLAND SEDIMENTS OF THE GREAT PLAINS

Major Field: GEOLOGY

Abstract: The purpose of this study was to identify the geologic signature of paleostorm events within the mid-continent region. This research aimed to create a better understanding of the long-term geologic history of major storms and to allow for better-informed projections regarding future return periods for such storms. The study locations were Cheyenne Bottoms Wildlife Refuge, Kansas and Canton Lake, Oklahoma. To determine the geologic signature of major storms, sediment cores were taken at both locations and sampled at high resolution (3 mm) intervals for grain size analysis using a Cilas laser particle size analyzer. Downcore chronology was determined through Pb-210, Cs-137 and C-14 dating methods. Using a recent known major storm occurrence at Canton Lake, the signature created by storms in the geologic record was identified. The resulting signature was then used to identify paleostorms in the longer-term record in the Cheyenne Bottoms core. The results were also used to determine storm/climate cycles in the long-term geologic record, and to calculate true return periods for major storms. A better understanding of true return periods and possible increases in frequency or intensity of large storms is essential in the effort to mitigate future damage to infrastructure and loss of human life

TABLE OF CONTENTS

LIST OF TABLES

Table Page

LIST OF FIGURES

Figure Page

CHAPTER I

INTRODUCTION

1.1 Objective

Paleotempestology, the study of long-term regional storm history from geological proxy evidence, allows us a unique opportunity to assess the frequency and intensity of major storms during the geologic past, well beyond the often brief historic record. Many scientists predict that the Earth's temperature will increase as a result of changes in atmospheric CO_2 and other trace gases (e.g., Houghton et al., 1990). As a result of the increasing temperatures, a change in the intensity and possibly the frequency of extreme atmospheric events (e.g. tornadoes, thunderstorms, hurricanes) is also projected to occur (Wigley, 1988).

Numerous publications have suggested the possibility of an increase in tropical cyclone activity under a global warming scenario (e.g., Emanuel, 1995; Emanuel, 2005; Elsner et al., 2011). Furthermore, research on global lightning frequencies by Price and Rind (1992) has shown a 5-6% for every 1°C temperature change. Moreover, some studies have projected an increase in frequency and intensity of catastrophic wind storms (e.g., Pearce, 1995; O'Hare 1999). There are, however, few published studies that examine how climate change might affect the occurrence of other cyclonic phenomena, such as tornadoes. The record of historical tornadoes extends back only to about 1880 (Grazulis, 1991). Therefore, the problem of determining the actual return periods of large catastrophic tornadoes is complicated by the scarcity of historic (and prehistoric) documentation.

Knowledge of paleo-tornado frequencies, extracted from the long-term records found in lake or wetland sediments, would be of great benefit in quantifying the return period risk of major catastrophic tornadoes in regions susceptible to such hazards. Many areas of the Great Plains states are currently at elevated risk of tornadoes. The studies by Wigley (1988), Price and Rind (1992) and White and Etkin, (1997) suggest that a warming future will bring an increase in the intensity and/or frequency of cyclonic storms. If a relatively warmer future increases the possibility of more intense and/or more frequent storms, a better understanding of the long-term record of convective storms will be of much benefit.

The purpose of this research was to develop a chronology of the occurrence of tornadoes over the past several millennia and therefore to provide an estimate of the frequency, and therefore the true risk, of intense windstorms. This study also aimed to quantify the relationship between climate change and tornado frequencies and to provide insight into the long-term history of tornadoes, which will be of significant value in predicting future changes in frequencies and intensities of tornadoes. The study used the following approach: 1) identify suitable locations to collect sediment cores, i.e., locations that have continuous or near-continuous deposition and which have experienced a relatively high frequency of tornadoes; 2) determine sedimentation rates for the select locations using ^{210}Pb, ^{137}Cs,and ^{14}C; 3) use the sediment core geochronology, along with knowledge of the known historic occurrence of tornadoes in the region, to determine the signature of such storms in the sediment record; 4) use the resulting storm signature to identify paleo-storms and determine storm/climate cycles in the long-term geologic record; 5) calculate the true long-term return periods of large tornadoes.

From 1950-1989, thunderstorm-related conditions (tornadoes, heavy rain, lightning, wind, and hail) caused $25.4 billion worth of damage, while wind storms alone caused $2.3 billion in damage in the United States (Changnon and Changnon, 1992). Future projection models provided to governments and weather prediction organizations, regarding possible

increases in the number and strength of future tornadoes, can be used to help protect human life and prevent property damage caused by these storms. The results of this study will, it is hoped, aid in that effort by enhancing our understanding of the geologic history of large catastrophic wind events and by quantifying the long-term return period of large and damaging storms.

1.2 Paleostorm Record in the Midcontinent

The Great Plains region has a highly diverse climate. There is a wide variation in temperature as well as moisture content throughout the different regions of the Great Plains (Figure 1). Many geographic factors add to this variability. There are mountains to the west, the Gulf of Mexico providing moisture from the south, and Arctic air coming from the north. In the warmer months, March to October, convective storms, including tornadoes, become a major factor.

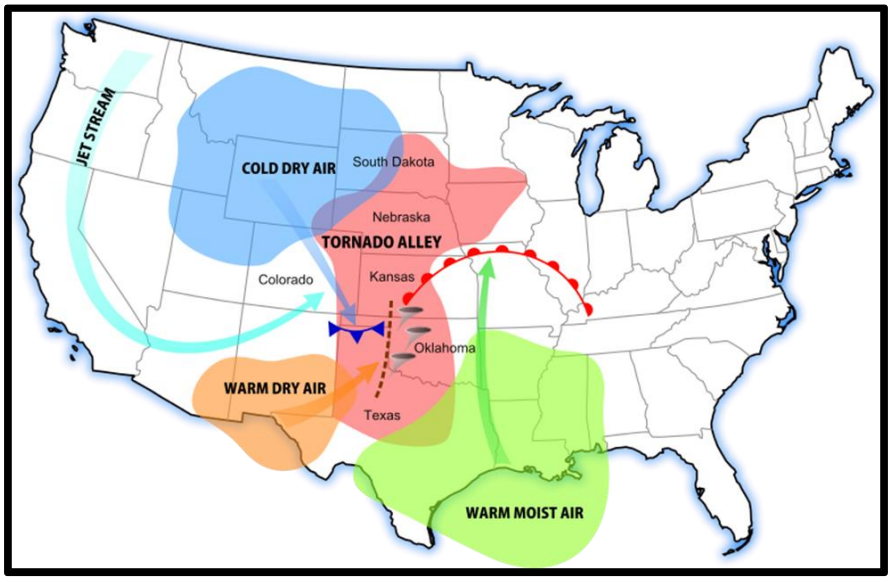

Figure 1: The "tornado alley" region of the United States, indicating the conditions that allow for the high frequency of tornadoes within the southern and Central Great Plains. Source: http://www.nssl.noaa.gov/primer/tornado/tor_climatology.html

The Great Plains region has the highest frequency of tornadoes in the world (NOAA/NWS, 2014). In the Great Plains from 1950-2013 there have been approximately 26,500 tornadoes,

accounting for an estimated 1,900 fatalities and 27,000 injuries. In Kansas alone, there have been approximately 4,000 tornadoes from 1950-2013 (NOAA/NWS, 2014a).

Much of the early work on tornado climatology in the United States was done by John Park Finley in his book *Tornadoes* published in 1887. The main difficulty with historical tornado records lies in the fact that for a tornado to be recorded it must be seen or observed by somebody. Unlike other events such as rainfall which can be measured with fixed instruments, a tornado is for the most part a brief and localized event. In the past the Great Plains region was not densely populated. Therefore not all tornadoes were documented and in turn the accuracy of any count of annual tornado occurrences cannot be trusted with the data currently available.

The National Climatic Data Center states that, in terms of absolute tornado counts per year, the United States is far above the rest of the world, averaging ~1000 per year, with Canada a distant second at ~100 per year. According to NOAA, 77% of tornadoes in the United State are considered weak (Enhanced Fujita-0 or EF-1), while 95% are below EF-3 intensity (National Climactic Data Center/NOAA, 2015). Moreover, only 0.1% of tornadoes in the United States reach EF-5 status. Taking into account that approximately 1000 tornadoes occur in the U.S. every year, 20 can be expected to be major (>EF-3) and 1 will likely be extreme (EF-5) (NCDC/NOAA, 2015). Because the historical record of smaller tornadoes might be skewed due to lack of documentation, when examining trends in annual tornadoes it is beneficial to consider the frequency of the major storms (>EF-3), which have a higher probability of being recorded even before the introduction of Doppler radar and modern meteorological tools. Figure (2) from NOAA/NWS shows the annual number of tornadoes larger than EF-3 from 1954 to 2012.

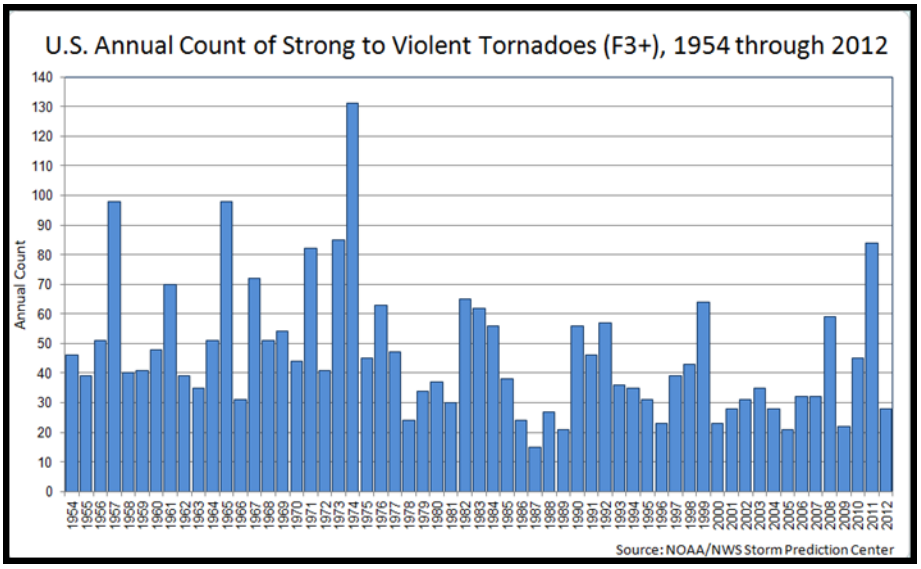

Figure 2: U.S. annual count of violent tornadoes (>EF-3), 1954 – 2012. There is a slightly decreasing trend in the occurrence of strong tornadoes during this period. Source: NOAA/NWS Storm Prediction Center

Many recent studies have attempted to determine how tornado frequency and intensity have changed with a varying climate but a consensus has not been reached. However, a new finding suggest tornadoes are peaking earlier in the season than before within the so-called tornado alley (Figures 3 and 4) (Long and Stoy, 2014). The study examined the 60-year database of the National Weather Service and found that peak tornado activity is occurring up to two weeks earlier than it did 50 years ago within the southern and central US Great Plains (Long and Stoy, 2014). Additionally, Greg Carbin, a meteorologist for NOAA, investigated the meteorological conditions required to produce tornadoes and found they are also occurring earlier in the year, confirming the results of Long and Stoy (2014). However, he noted that a problem arises when studying trends in tornado activity: "There are no proxies in the geologic record for tornadoes; eyewitness are needed" (Morton, 2015). One of the goals of this study was to create a proxy for identifying the geologic signature of tornadoes. A proxy would reduce the need for an

eyewitness to record the storm and would allow for better analysis of trends in tornado frequency and intensity in a given area.

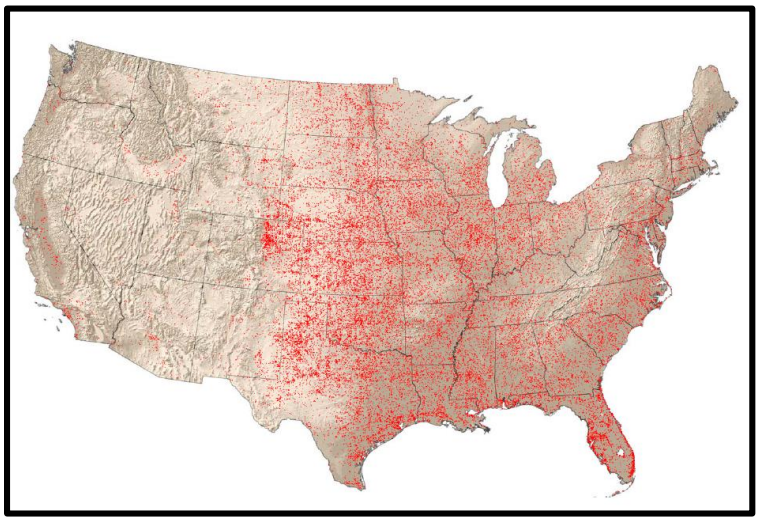

Figure 3: Occurrence of tornadoes across the United States from 1954 – 2009, indicated by red dots (Long and Stoy, 2014)

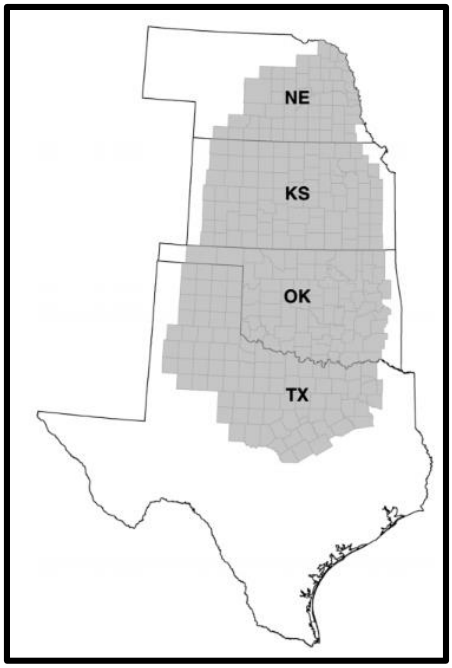

Figure 4: Region of the Great Plains with the highest tornado frequency (Long and Stoy, 2014).

1.3 Study Areas

1.3.1 Cheyenne Bottoms, Kansas

The study areas chosen for this study had to meet certain criteria. They needed to be located in an area of continuous or near-continuous deposition and a high frequency of tornado occurrence. Cheyenne Bottoms, located centrally in Kansas as well as the Great Plains region, is a basin-like feature that is approximately 166 km^2 in area (Figure 5) (Latta, 1950; Bayne, 1977; Fredlund, 1992). Cheyenne Bottoms is located in an internally drained structural basin (Latta, 1950; Bayne 1977). Loess deposits, both pre-Wisconsin and Wisconsin, separate the basin from the Arkansas River to the south (Fredlund, 1992). Sand dunes of unknown age lie to the east, whereas outcrops of Cretaceous-age sandstone, limestone, and shale bedrock flank the west and north sides of the basin (Fredlund, 1992). Due to the importance of Cheyenne Bottoms to migratory waterfowl, artificial management of the hydrology of the area was incorporated in the early 1950s by the construction of dikes throughout the wetland region (Fredlund, 1992).

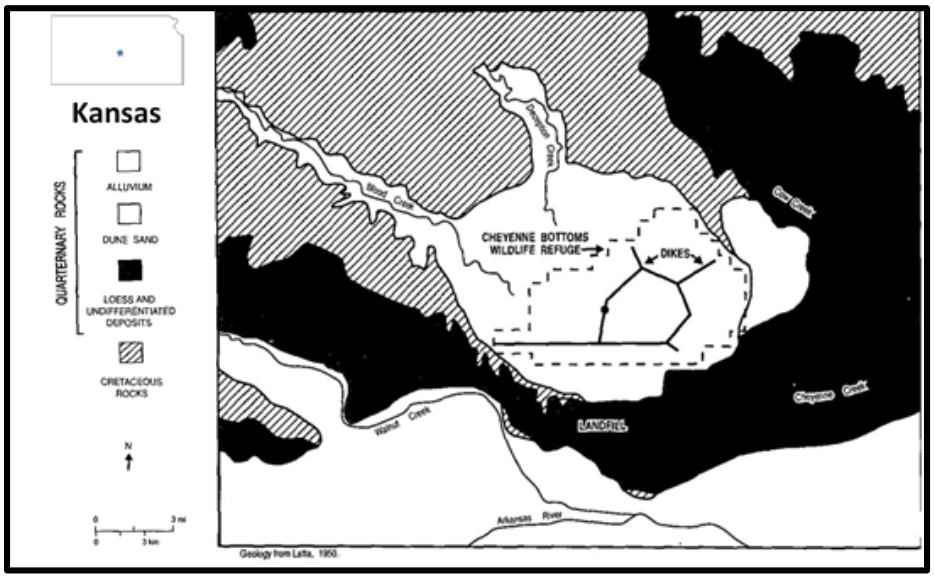

Figure 5: Geology of Cheyenne Bottoms, Kansas and surrounding area. Blue star on inset map shows approximate location of Cheyenne Bottoms Wildlife Refuge. Figure modified from Fredlund (1992).

The late Cenozoic climate history of Cheyenne Bottoms was described by Fredlund (1992), based on pollen analysis of samples from a borehole in the wildlife refuge. The four major chronological periods identified (Farmdalian, Woodfordian, Woodfordian – Holocene Transition, and the Holocene) were examined for climate trends, using sediment and pollen analysis. According to Fredlund (1992) between 30,000 and 24,000 yr BP., grassland – sage steppe dominated the regional uplands surrounding the basin, culminating with a basin wide drying cycle from 25,000 to 24,000 yr BP. The Woodfordian climate varied from cold xeric conditions from 24,000 to 16,000 yr BP to cooler and more mesic conditions from 16,000 to 12,000 yr BP (Fredlund, 1992). The Holocene had three distinctive periods: the early Holocene (9,700 to 8,500 yr BP), the mid-Holocene (8,500 to 4,800 yr BP), and the late Holocene (4,800 yr BP to present) (Fredlund, 1992). The early and late Holocene climates were characterized by increased aridity and fluctuations in water levels within the basin, while the mid-Holocene showed signs of a more stable water level (Fredlund, 1992).

Cheyenne Bottoms was selected as the study locality due to its potential for continuous, uninterrupted deposition of late Quaternary sediments as evidenced by its geologic history (Latta, 1950; Bayne, 1977; Fredlund, 1992). Additionally, according to the National Weather Service (NOAA/NWS, 2014), from 1950-2013 there have been 96 tornadoes reported in Barton County, Kansas, therefore meeting the second requirement of the study location by historically having a relatively high frequency of tornadoes (Figures 6 and 7)

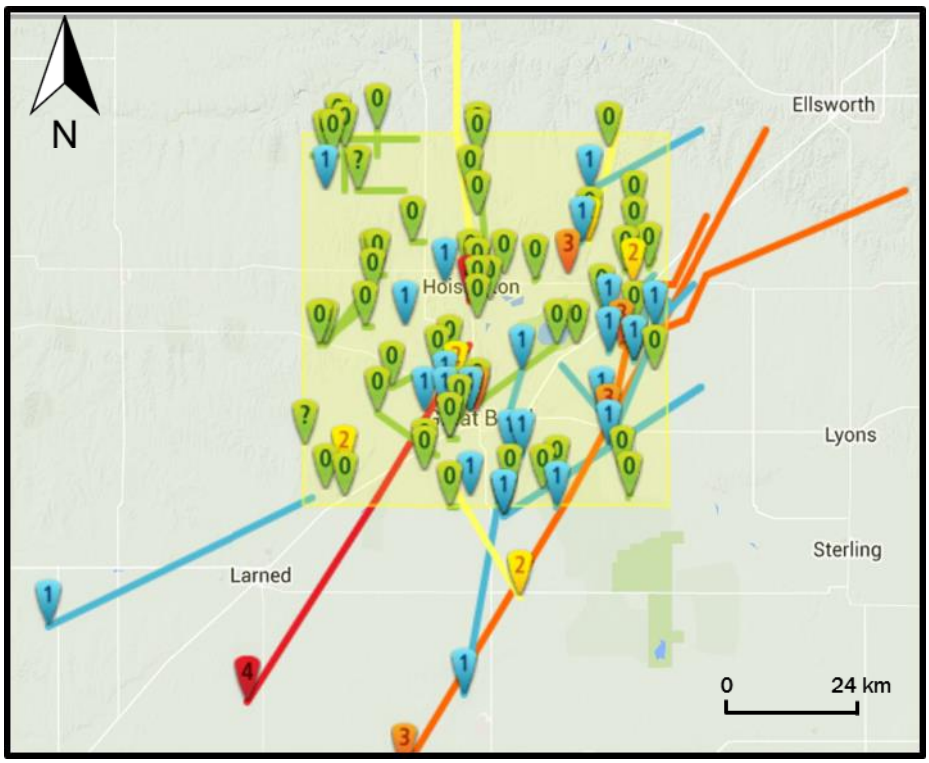

Figure 6: Tornado occurrence in Barton County, Kansas, 1950-2013. County boundaries are outlined in yellow. Symbols indicate magnitude on the Fujita Scale. Image from tornadohistoryproject.com (NOAA/NWS, 2014).

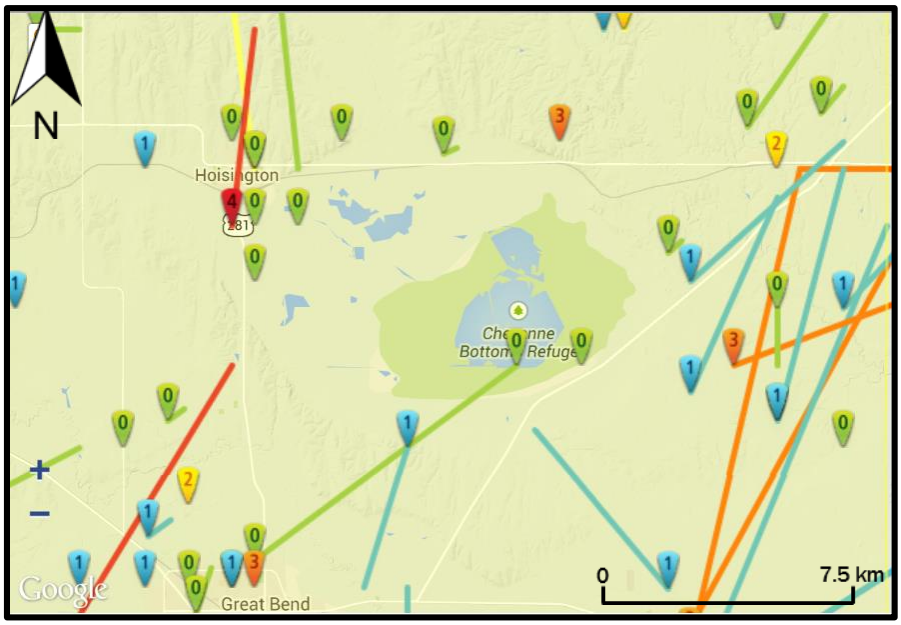

Figure 7: Cheyenne Bottoms Wildlife Refuge showing tornadoes that occurred in close proximity to the study location. Paths are shown for recent tornadoes along with magnitude on the Fujita Scale from 1950-2013. Image from tornadohistoryproject.com. (NOAA/NWS, 2014)

1.3.2 Canton Lake, Oklahoma

The second location for this study was Canton Lake, OK. Canton Lake is located about 98 miles Northwest of Oklahoma City, OK. Canton Lake was created in 1948 when the Canton Dam was constructed to provide drinking water as well as flood risk management for Oklahoma City.

Canton Lake was chosen because of a known storm occurrence. The NOAA/SPC recorded a tornado crossing the lake on May 24, 2011 with a magnitude of EF-3 (Figure 8) (NOAA/NWS, 2014). This violent storm was used to identify the geologic signature of tornadoes in the geologic record. In Oklahoma there have been approximately 3,500 tornadoes since 1950 and 13 tornadoes around Canton Lake (NOAA/NWS, 2014) (Figure 9).

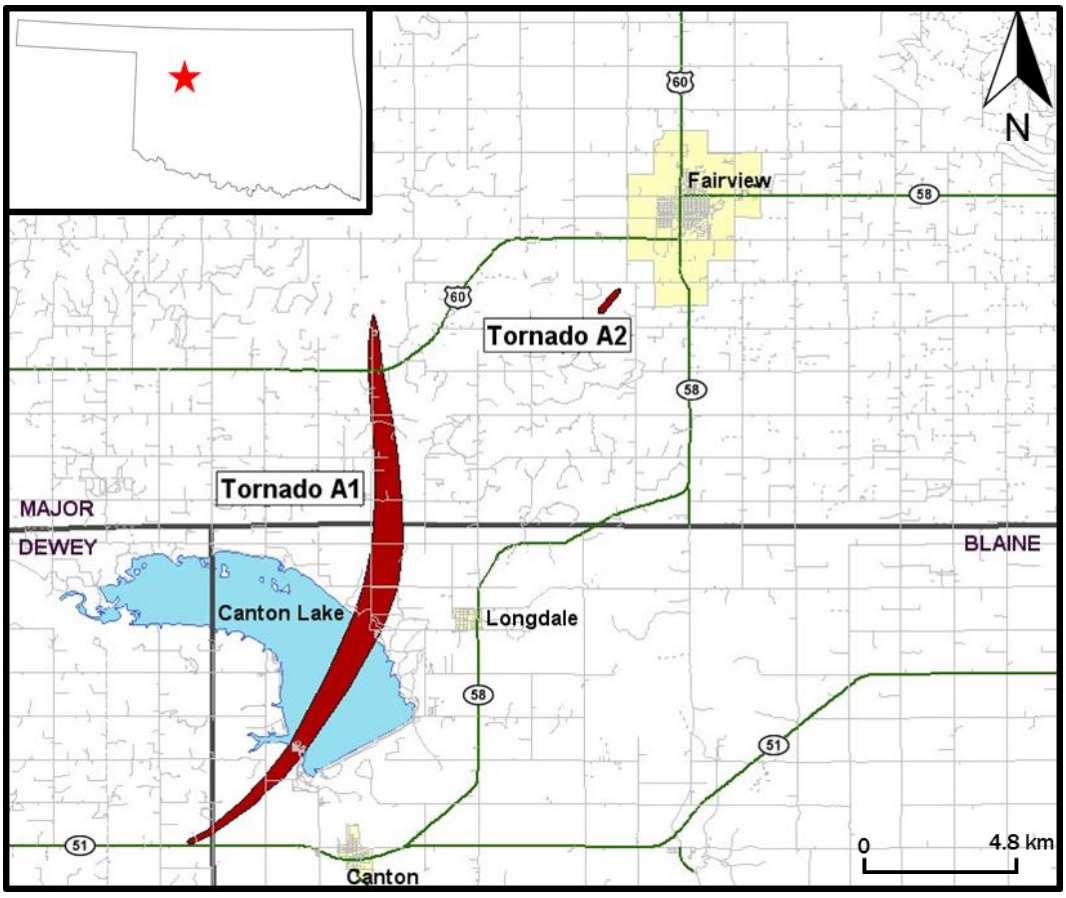

Figure 8: Path of May 24, 2011 tornado, labeled tornado A1, which traveled directly through Canton Lake, OK. The path of the tornado is shown in red NWS (2014)

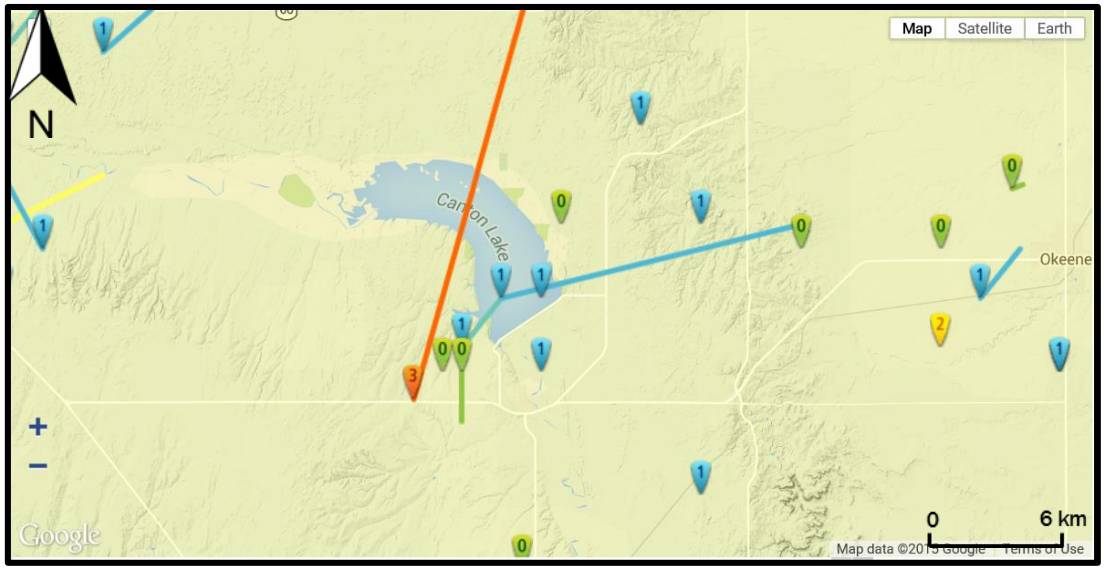

Figure 9: Canton Lake, OK region, showing the Fujita Scale magnitude of tornadoes from 1950-2013. Image from tornadohistoryproject.com (NOAA/NWS, 2014).

1.4 Previous Work

Paleotempestology has typically been focused on the study of tropical cyclone activity through geologic time (e.g., Liu and Fearn, 1993; Liu and Fearn, 2000; Boose et al., 2001; Nott, 2004; Coor, 2012). These paleostorm studies were conducted in coastal lakes and wetlands because they provided a continuous record of sedimentologic events at or near the coast. A variety of methods have been used to quantify these paleostorms, including: counting of overwash sand layers in sediment cores, ground penetrating radar surveying, micropaleontology, and stable isotope geochemistry (Liu and Fearn, 1993; Liu and Fearn, 2000, Hassan et al., 1997; Nott, 2004; Lamb, 2005; Coor, 2012; Das et al., 2013).

There have been few studies investigating how climate change will affect cyclonic windstorms. Wigley in (1988) proposed that, as a result of increasing temperatures, a change in intensity and/or frequency of extreme atmospheric events (tornadoes, hurricanes, thunderstorms, e.g.) should be expected. Scientific consensus for the effect of global warming on extreme events is summarized in Table 1.

Table 1: Scientific consensus on climate warming and its possible effects on extreme events, Modified from White and Etkin (1997)

Hazard	Trend with Climate Warming
Tropical Cyclone	More Frequent
Convective Storms	More frequent and severe
Heat Waves	More frequent and severe
Cold Waves	Less frequent
Floods	More frequent
Drought	More frequent, possibly prolonged

Among others, emergency management agencies and the risk management industry have a strong interest in developing a better understanding of how climate change will affect storm frequency (Friedman, 1988; Berz, 1993; Pearce, 1995; White and Etkin, 1997). According to Berz (1993), an increase in convective processes will increase the frequency and severity of tropical cyclones. Moreover, if warmer mid-latitude climates enhance levels of convective storms, then an increase in frequency and perhaps intensity of tornadoes would be expected (Peterson, 1999). This hypothesis has been examined by Etkin (1995), who investigated how tornadoes responded to warmer climates in Western Canada. Etkin (1995) found a correlation between tornado occurrences and mean monthly temperature anomalies, indicating that tornado frequency and temperature are correlated.

An example from a recent study on Holocene sea level change (McNabb, 2014) is illustrated in Figure 10. Using grain size parameters such as percent sand, mean grain size, and others, along with a history of known storm events, a sedimentologic signature for periods of increased storm frequency was identified. These same proxies and methodologies have been applied in the current study to interior water bodies to determine the frequency of tornadoes dating back several millennia.

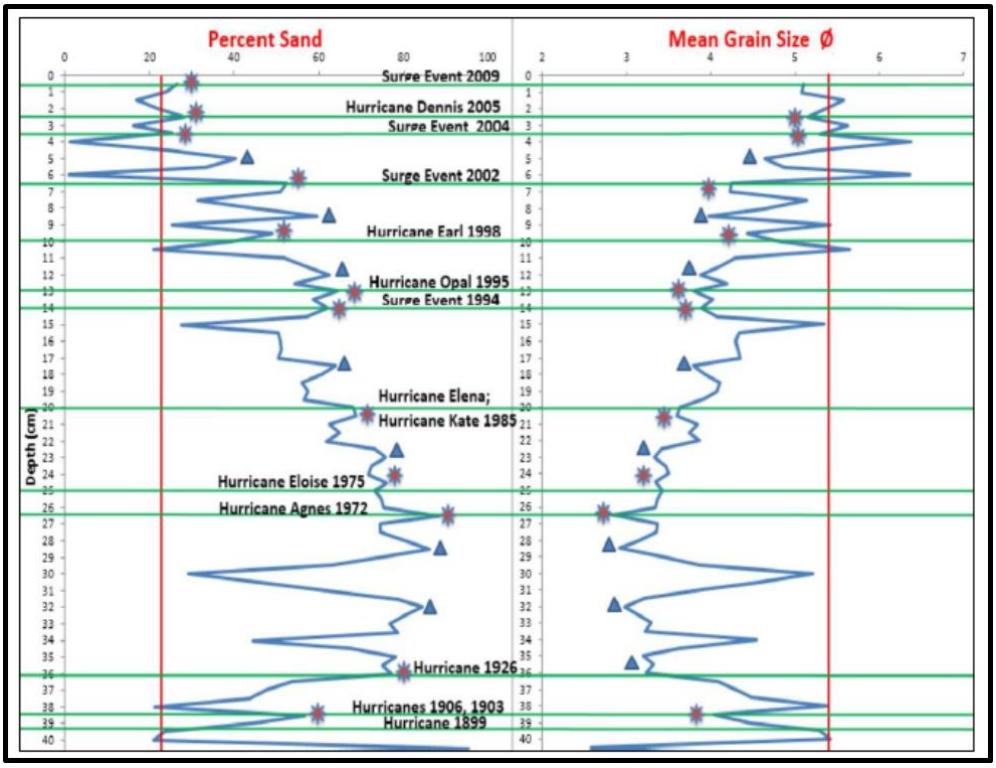

Figure 10: Example of paleostorm analysis of a sediment core taken from Oyster Pond, St. Vincent Island, on the northwest coast of Florida. The green horizontal lines and asterisks represent specific known hurricane events, based on core chronology, and the blue triangles are false positives. Figure from McNabb (2014).

The number of tornadoes reported in the United States per year has increased by approximately 14 per year over the past half century (Diffenbaugh, et al., 2008). Changes in tornado activity can be explained by changes in the mean jet stream position associated with the El Niño–Southern Oscillation (Cook and Schaefer, 2008). There is a potential for global warming to affect the frequency and distribution of tornadoes. The extreme thunderstorms that spawn tornadoes originate in a larger-scale environment characterized by large vertical wind shear and convective available potential energy (CAPE) (Brooks et al., 2003). Generally, global warming is expected to increase CAPE by increasing temperature and humidity within the atmospheric boundary layer while simultaneously weakening vertical wind shear by decreasing the pole-to-equator temperature gradient (e.g., Trapp et al., 2007a). Regions that experience peak tornado

occurrence at present could therefore see reductions due to weakened shear. However, these reductions could be offset by increased CAPE, which could lead to increased tornado occurrence (Diffenbaugh, et al. 2008).

Several studies have examined future trends in severe thunderstorms and tornadoes. One approach has been to examine the relationship between increased greenhouse gases and tornado frequency. Using this approach several studies have concluded that as a result of increased greenhouse gases, severe thunderstorms are likely to increase as well (Del Genio et al., 2007; Marsh et al., 2007; Trapp et al., 2007a).

In a study by Elsner et al. (2013), a statistical process model was used to simulate the spatial occurrence of nonviolent tornadoes and to predict the distribution of the rare, violent tornadoes that occur during the spring across the US central Great Plains. The results from that study are as follows: the average rate of nonviolent (wind speed < 70 m s^{-1}) tornadoes are 55 per 104 km^2 for the 62-year period. This can be compared with an average rate of only 1.5 violent (wind speed > 90 m s^{-1}) tornadoes per 104 km^2 over the same period (i.e., less than 3 % of all tornadoes). Violent tornado report density peaked at 2.6 per 104 km^2 (over a 62yr period) in urban areas but was only 0.7 per 104 km^2 in the countryside.

Elsner et al. (2014) conducted a study whose aim was to determine tornado intensity from damage path dimensions. They examined tornado paths from 2007 - 2013. They found a distinct relationship between the intensity of the tornado on the EF scale and its damage path dimensions (Figure 11 and Table 2). The damage path width increases as the intensity of the storm increases. The model also indicates a 25% increase in expected intensity over a threshold intensity of 29 m/s for a 100 km increase in path length (Elsner et al., 2014). Using the Elsner et al. (2014) model, given a known intensity and an estimated damage path width, storms can be selected based on their proximity to the study location and therefore their ability to influence the sediment texture data of the region.

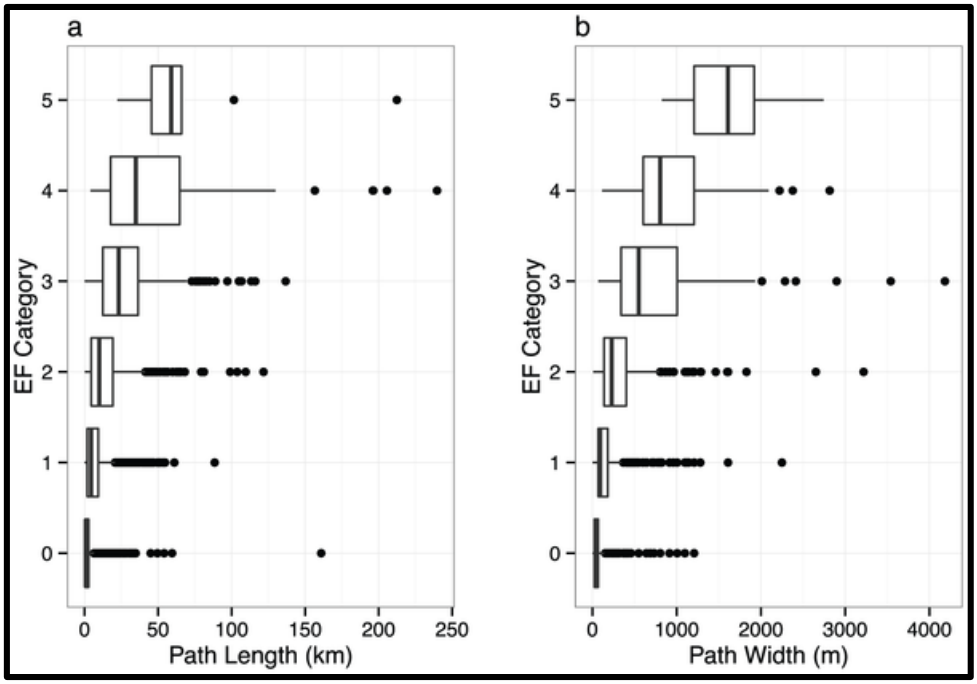

Figure 11: Box plots of damage path length (a) and damage path width (b) for EF categories, indicating a positive relationship between storm intensity and the length width of the damage path (Elsner et al., 2014).

Table 2: The derived EF scale and corresponding wind speed ranges based on three-second gusts. Data are based on all reported tornadoes in the United States (2007–2013). N is the sample size. The lower and upper quartile values are given in parentheses (Elsner et al., 2014).

Category	**Wind Speed**	**N**	**Length (km)**		**Width (m)**	
	($m\ s^{-1}$)		Mean	Median	Mean	Median
EF-0	29 - 38	4994	2.27	0.80	54.90	45.70
EF-1	28 - 49	2642	7.10	4.39	163.80	91.40
EF-2	49 - 62	818	14.29	10.03	344.10	228.60
EF-3	62 - 75	232	29.09	23.28	736.30	548.60
EF-4	75 - 89	57	52.55	34.84	997.90	804.70
EF-5	89 - 105	9	71.95	58.95	1635.80	1920.20

1.5 Hypotheses

Previous studies of convective storms have only had the ability to examine tornado records going back about 150 years at most, with the reliability of the record diminishing significantly with age (Grazulis, 1993; Peace, 1995; O'Hare, 1999). This study used the most reliable historic tornado database (NOAA/NWS, 2014a). This database includes tornado records from 1950 to 2013.

A record this brief (63 years) does not allow for the accurate determination of true storm return periods, and provides limited insight as to how tornado frequencies might change due to a warming climate. This investigation has the potential to lengthen the tornado record by several millennia. This extended history of tornadoes will allow for a more robust prediction of true return periods for these large storms and a better understanding of how tornado frequency might change with a changing climate.

This investigation tested the hypothesis that the historic record of extreme events like tornadoes is not a reliable indicator of the long-term occurrence of such storms. A corollary hypothesis was that, in sediments from long-lived lakes and wetlands, a geologic signature of storms, whether sedimentologic, geochemical, or both, can be detected. That signature, when combined with a chronology, can be used to better understand the long-term pattern of occurrence of major storms, and to make better-informed projections regarding future return periods for such storms. This investigation also tested the hypothesis that extreme events like tornadoes have increased in frequency during warm periods in the geologic past. This research sought to develop a chronology of the occurrence of tornadoes over the past several millennia and therefore provide an opportunity to estimate the frequency, and therefore the true risk, of intense windstorms. This insight into the true long-term history of tornadoes will be of significant value in predicting future changes in frequencies and intensities of tornadoes

CHAPTER II

METHODOLOGY

2.1 Field Sampling

A total of four cores were taken, two at Cheyenne Bottoms, Kansas and two at Canton Lake, Oklahoma. The Cheyenne Bottoms cores (041014-01 and 041014-02) were extracted using a vibrocore system (Figure 12). Aluminum tubes of 7.62 cm (3 in) diameter were used for core collection. The Canton Lake cores (051914-01 and 051914-02) were obtained using a hand-held push corer to prevent the lake sediment from being disturbed or homogenized (Figure 13). Clear CAB tubes with a diameter of 5.08 cm (2 in) were used for core collection.

2.2 Core Preparation

One core from each site, 041014-02 from Cheyenne Bottoms and 051914-02 from Canton Lake, was chosen for sedimentologic analyses. The others cores were archived. The cores were split lengthwise, with half of the core used for analysis, and the remaining half retained in cold storage as an archive. The first core (041014-02), measuring 104.5 cm from Cheyenne Bottoms and sampled at a 0.3 cm interval for the top 76 cm and then sampled at a 0.5 cm interval to the bottom of the core (Figure 14). The second core (051914-02), measuring 76 cm from Canton Lake was sampled at a 0.5 cm interval.

2.3 Sediment Texture Data

A CILAS 1180 laser particle analyzer was used for analyzing sediment textural parameters. The CILAS was employed to determine grain size in phi units (Ø), percent sand, percent silt, percent clay, moment skewness, and moment standard deviation, along with the grain diameters (in micrometers) at significant percentiles in the cumulative curve (5%, 7%, 10%, 16%, 50%, 84%, 90%, 95%, and 98%).

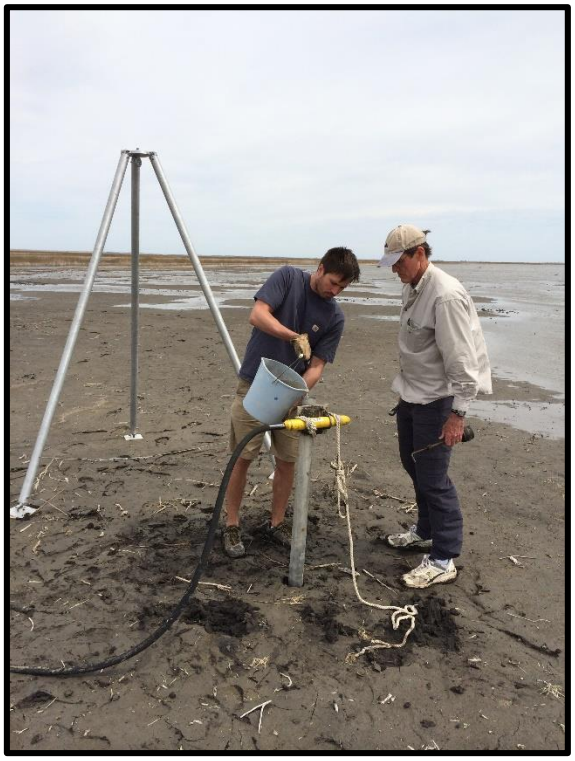

Figure 12: Vibrocore extraction from Cheyenne Bottoms, Kansas

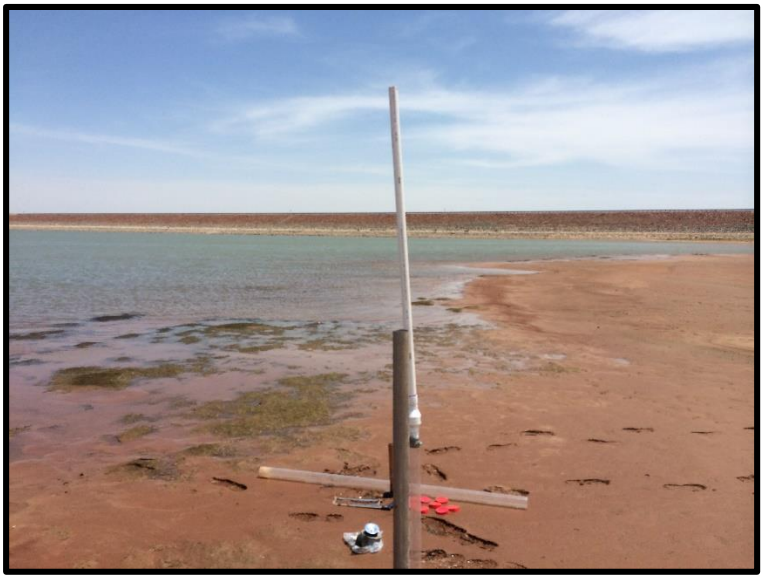

Figure 13: Extraction of push core from Canton Lake, OK.

Figure 14: Split core 041014-02 from Cheyenne Bottoms, Kansas that was used for sediment and chronologic analysis. Core measured 104.5 cm long.

Samples for the size analysis were placed in pre-weighed plastic dishes, weighed, dried for 48 hours in an oven at 65°C, and weighed again after cooling to determine the bulk dry weight of the sample. Once removed from the oven, samples were ground up into a fine powder using a mortar and pestle to remove any clumps of sediment remaining. Next, approximately 2 grams of each sample were placed in 200 mL beakers along with ~100 mL of dispersant (de-ionized water and 0.5% sodium hexametaphosphate) and stirred using a magnetic stirrer. While being actively stirred and in suspension, approximately 15 mL of sample was removed by pipette and injected into the CILAS reservoir for textural analysis. The grain size statistics were then determined using the Folk (1974) statistical methods.

Each sampled interval was run at least twice through the CILAS grain size analyzer. This procedure was implemented in order to achieve repeatable results. For the most part samples needed to be only run twice. However, some samples were run three or four times until the sample results were found to be repeatable. Once the two textural data sets for each sample were collected, they were averaged, resulting in 212 averaged pairs for the Cheyenne Bottoms core and 160 averaged pairs for the Canton Lake core. All data parameters were displayed in profile plots.

For analysis of the CILAS sediment textural data a geological and geophysical modelling program, Geosoft Oasis Montaj, was used to create a surface plot that represented the histogram percent of grain sizes in phi units present in each segment of the core. The particle size distribution (PSD) plot allowed for identification of small changes in the sedimentology of the Cheyenne Bottoms core.

2.4 Geochronology

Core geochronology was established using a combination of ^{210}Pb, ^{137}Cs, and C-14 dating methods (Stanners and Aston, 1981; Olsen et al., 1982; Chanton et al., 1983; Huntley et al., 1985; Milan, 1995; Kirchner and Ehlers, 1998). ^{210}Pb, with a 22.3 year half-life, bonds to clay minerals,

fine silts, and humic materials (Olsen et al., 1982; Chanton et al., 1983; Kirchner and Ehlers, 1998) and is used for dating lake sediments. The dating method assumes that the annual atmospheric flux of ^{210}Pb, produced by the decay of 222-Rn, has been relatively constant over time (Appleby and Oldfield, 1978; Kirchner and Ehlers, 1998; Walker, 2005).

^{137}Cs has a half-life of approximately 30 years, and is an artificial fission product that occurs in the atmosphere primarily as a result of nuclear weapons testing in the 1950's and 1960's. First entering the atmosphere in 1954, atmospheric concentrations of ^{137}Cs peaked at the time of the Nuclear Test Ban Treaty in 1963 (Kirchner and Ehlers, 1998; Walker, 2005), and rapidly declined in the following decades (Kirchner and Ehlers, 1998). Cesium, like lead, adsorbs to clay minerals, silts, and humic materials (Stanners and Aston, 1981; Milan et al., 1995; Kirchner and Ehlers, 1998). The earliest occurrence of this isotope in a sediment core profile is generally taken to represent 1954, the year when it became commonly present in the atmosphere. A subsurface peak indicates 1963, a time-stratigraphic horizon for the peak year of atmospheric testing (Olsson, 1986; Kirchner and Ehlers, 1998; Walker, 2005).

Thirty-three samples were collected for ^{210}Pb and ^{137}Cs analysis from the Cheyenne Bottoms core. The sampling interval was 0.9 cm. This interval resulted from combining three samples from the CILAS analysis which were sampled at 0.3 cm each. The three samples were homogenized, placed in plastic petri dishes, and wrapped in electrical tape. This was done in order to allow the short-lived daughters of the radiogenic isotopes to accumulate and be contained in the vial for counting. Samples were set aside for a minimum of two weeks to let the parent isotopes of ^{210}Pb reach equilibrium. The samples were then placed on a High-Purity Germanium (HPGe) gamma detector for 48 hours or more depending on the activity of the sample. Gamma ray spectrometry was conducted and analyzed following a method similar to that of Kim and Burnett (1983).

For the Canton Lake core, the sampling interval was 1 cm through the whole core, resulting in 74 total samples. Once samples were collected, the samples were subjected to the same analytical procedure as the Cheyenne Bottoms core samples.

In order to establish the longer-term chronology for the Cheyenne Bottoms core, radiocarbon dates were obtained from organic matter in the sediment. During sample collection, two 1 cm thick sediment samples, at 77 cm and 99 cm depth downcore, were placed in a pre-weighed dish, weighed, dried in an oven overnight at 65°C, weighed after cooling, ground into a powder for homogeneity, and placed in a pre-weighed and labeled glass vial. Vials were sent to The National Ocean Sciences Accelerator Mass Spectrometry Facility (NOSAMS) at Woods Hole Oceanographic Institute for radiocarbon analysis.

CHAPTER III

RESULTS

3.1 Sediment Texture Data

Data obtained from the CILAS laser particle analyzer are shown in Figure 15 and 16. Particle sizes are shown in phi units (Ø), where:

$$Ø = -log_2 d$$

and d is the grain diameter in millimeters. Therefore a large phi size represents a smaller mean grain diameter. Mean grain size, standard deviation of mean grain size, percent sand, diameter in µm at the 5^{th} 10^{th} and 90^{th} percentiles, and the moment skewness were all used to aid in determining periods of increased or decreased storminess. The data sets are shown in Appendix A.

3.1.1 Cheyenne Bottoms

Mean grain size ranged from 5.24 Ø to 6.81 Ø with a mean of 6.02 Ø and therefore in the coarse silt to fine silt range (Wentworth, 1922). Percent sand values range from 0% to 13.14%, with a mean of 3.69%. There is a direct relationship between percent sand and mean grain size. As percent sand decreases the mean grain size increases, as seen in Figure 15. Standard deviation of mean grain size, the average diameter in µm at 5%, 10%, and 90%, and the moment skewness were also examined. Percent sand and mean grain size were considered the best textural parameters for the paleostorm model and were focused on for identification of periods of increased or decreased storminess. To remove trends in the data and allow for better peak

recognition downcore differences were calculated from adjacent samples, as reflected in Figure 15. By counting peaks in both the percent sand and mean grain size variation profiles, 13 significant peaks can be discerned in the mean grain size profile and 22 peaks in the percent sand profile (percent sand greater than + 1 standard deviation. above the mean)(Mean Grain Size – 1 standard deviation below the mean) (Figure 15).

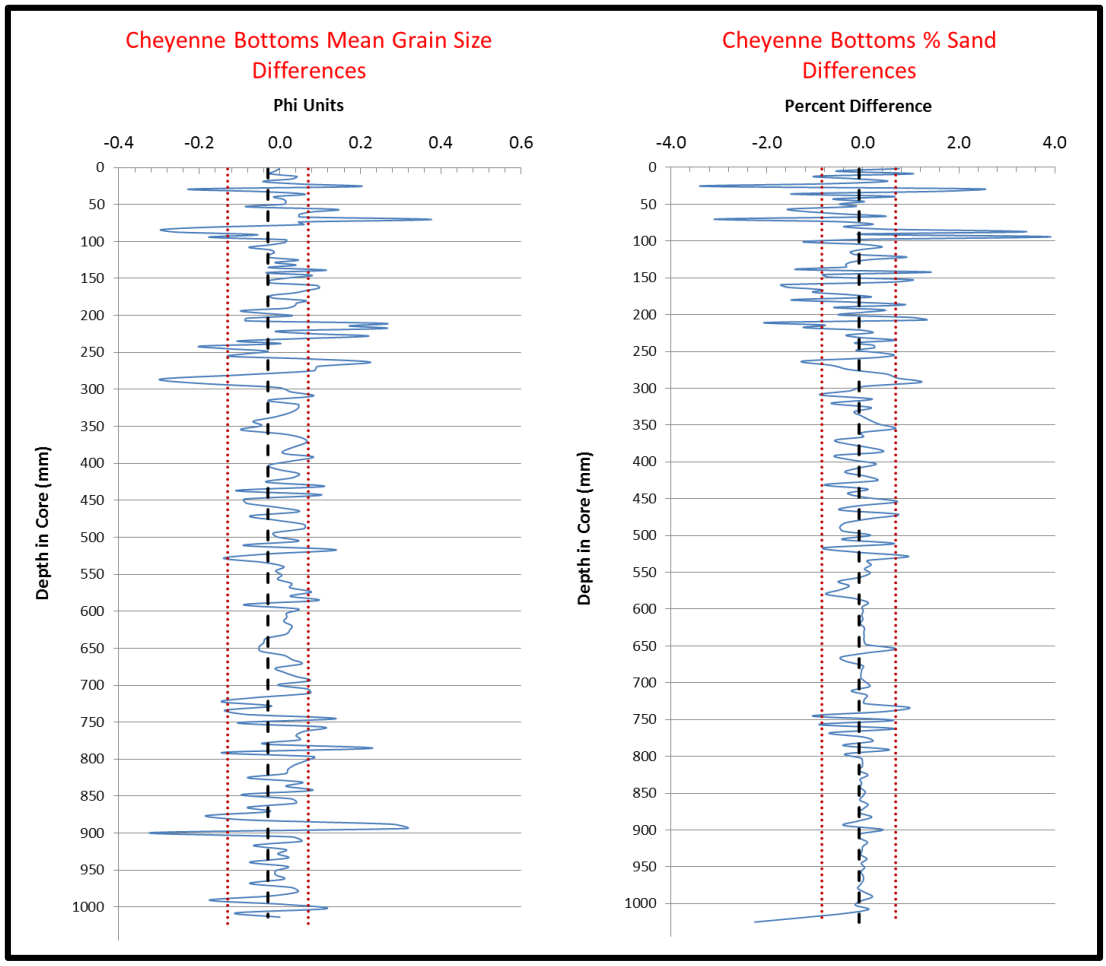

Figure 15: Results of sediment analysis for the 041014-02 core from Cheyenne Bottoms. Black dashed lines represent means for each parameter. Red dotted lines represent one standard deviation from the mean. Total core length is 104.5 cm

3.1.2 Canton Lake

The Canton Lake core is different from the Cheyenne Bottoms core. There was a much larger range in values for many of the textural parameters. This range could be due to a larger influence of recent storms around the Canton Lake region.

The Canton Lake core had percent sand values ranging from 0% to 75%, with a mean of 47.9%. For comparison, the mean percent sand from Cheyenne Bottoms was only 3.69%. Furthermore, there are significant changes, positive and negative, in the values of percent sand throughout the core, providing evidence of changes in energy within the system. Mean grain size ranges 3.52 Ø to 6.33 Ø, with a mean of 4.4 Ø and therefore represents a range from very fine sand to medium silt on the Wentworth scale. The average grain size from Canton Lake is also much larger: 4.4 Ø compared to 6.02 Ø in Cheyenne Bottoms. This is a result of the larger percentage of sand in the core. Just as in the Cheyenne Bottoms core, standard deviation of mean grain size, the average diameter in µm at 5%, 10%, and 90%, and the moment skewness were analyzed. Similarly, percent sand and mean grain size were found to be the best textural parameters for the paleostorm model and were focused on for identification of periods of increased or decreased storminess. To remove trends in the data and allow for better peak recognition downcore differences were calculated from adjacent samples, as reflected in Figure 16. By counting peaks in both the mean grain size and percent sand variation profiles, 15 peaks were identified in the percent sand profile and 5 peaks in the mean grain size profile (percent sand greater than + 1 S.D. above the mean) (mean grain size – 1 S.D. below the mean) (Figure 16).

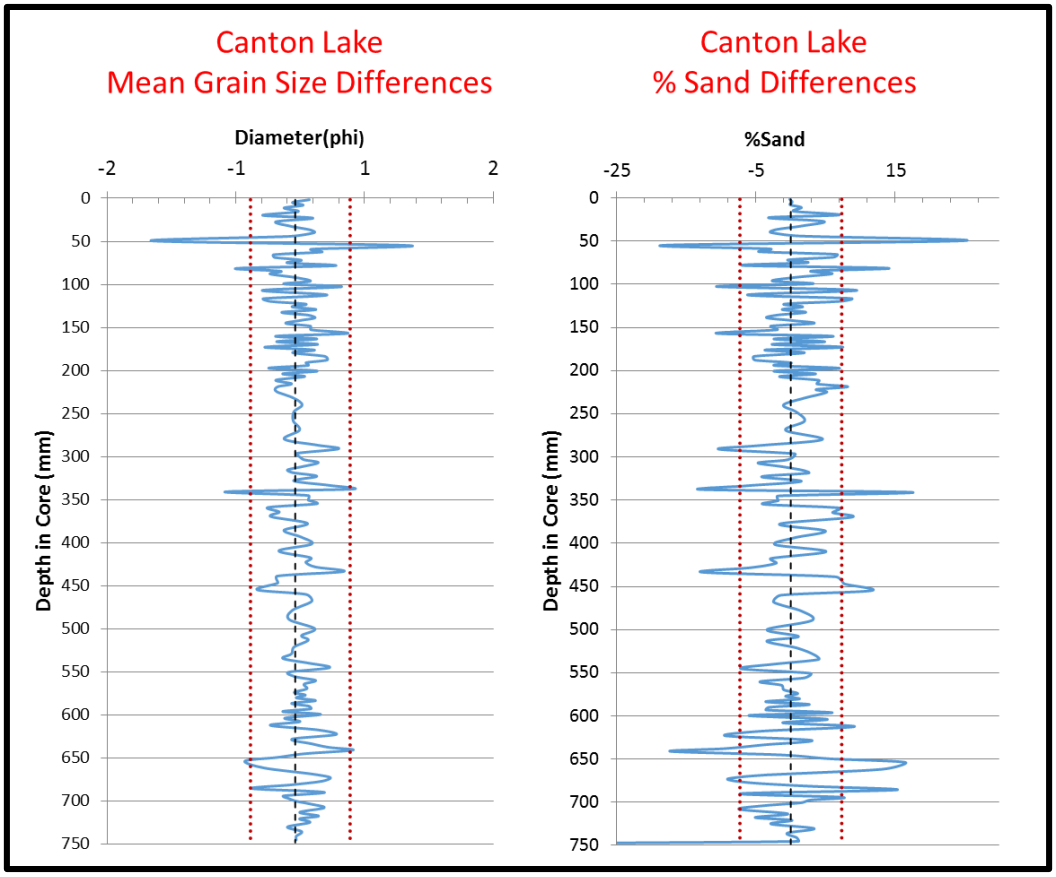

Figure 16: Results of sediment analysis for Core 051914-02 from Canton Lake. Dashed black lines represent means for each of the parameters. Red dotted lines represent one standard deviation. Total core length was 76 cm.

3.2 Core Chronology

3.2.1 Cheyenne Bottoms

In order to establish core chronology, ^{210}Pb dates were determined for the upper 41 cm. The lowest date identified from the ^{210}Pb analysis was 1891 at approximately 40 cm (Figure 17). The sedimentation rate decreases down core and therefore while the upper 25 cm ranges from 1.34 - 0.5 cm/yr the lower 25 – 41 cm is slightly slower at 0.47 – 0.29 cm/yr (Figures 17 and 18).

Below 41 cm two radiocarbon dates were acquired. Firstly, at 77.5 cm an age of 4918 +/- 44 cal yr BP and then at 99.5 cm an age of 5705 +/- 45 cal yr BP were obtained from organic mud

(Figure 19). The average sedimentation rate for the upper 40 cm was 0.316 cm/yr, from 40 – 78 cm the rate was 0.008 cm/yr, and below 78 a rate of 0.03 cm/yr (Figure 19).

Four dates and their corresponding depths were used to construct an age-depth plot for the Cheyenne Bottoms core. The dates are represented in calibrated years before the sampling date of 04-10-2014. The points are: sampling date 0 cal yr BP at 0.0 cm, the ^{210}Pb date of 124 cal yr BP, and the two C-14 dates at 77.5 cm and 99.5 cm of 4983 cal yr Bp and 5770 cal yr BP (Figure 19). The radiocarbon dates were converted using the CALIB 7.1 calibration scheme. This age-depth plot was used to determine the age at any depth downcore and therefore the date of specific events in the sediment record of Cheyenne Bottoms, Kansas.

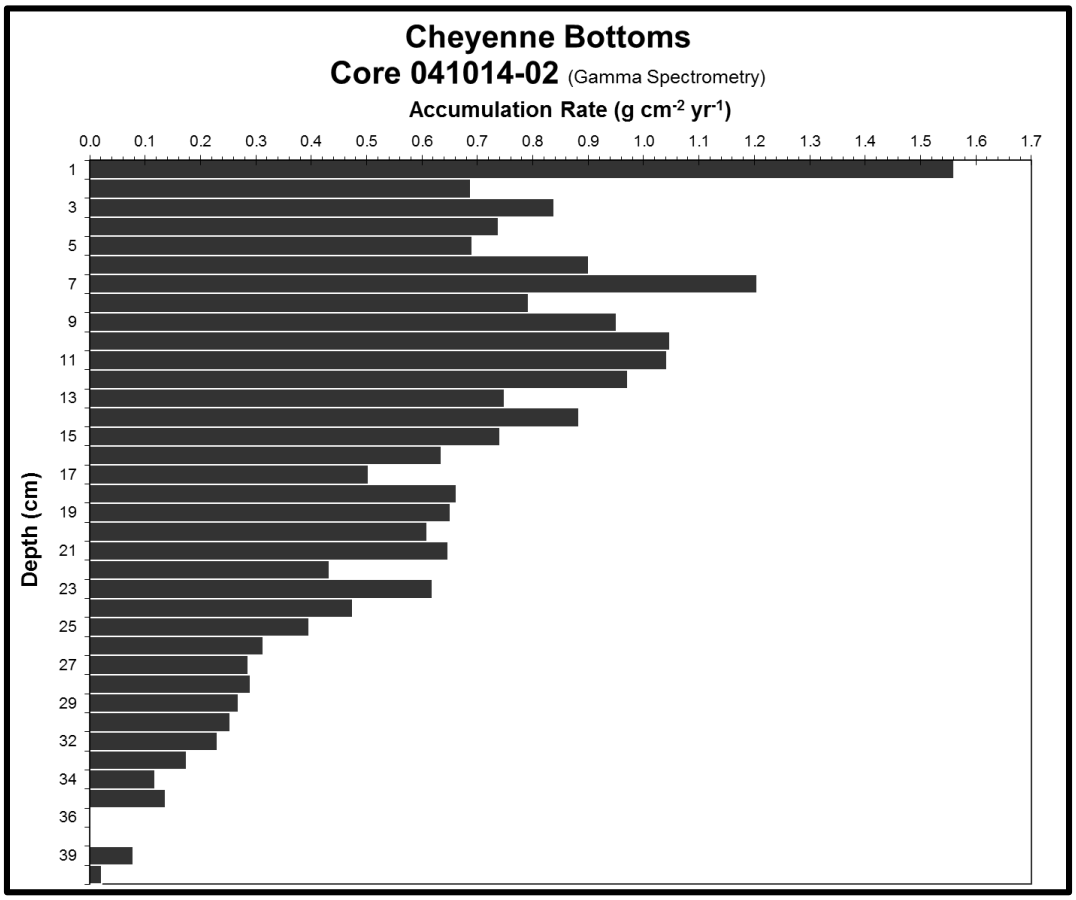

Figure 17: Sediment Accumulation rate vs. depth for the Cheyenne Bottoms core, based on ^{210}Pb analysis

^{137}Cs was also analyzed, via gamma spectrometry, in order to better determine the core chronology. The first appearance of ^{137}Cs in the atmosphere, due to nuclear testing, occurred in the early 1950s. The first appearance of ^{137}Cs downcore occurs at about 32 cm. This is in reasonably good agreement with the ^{210}Pb chronology, which produced a date in the late 1940s for that horizon. The peak concentration of ^{137}Cs in the atmosphere is generally taken to correspond to 1963 A.D., when peak nuclear testing occurred.

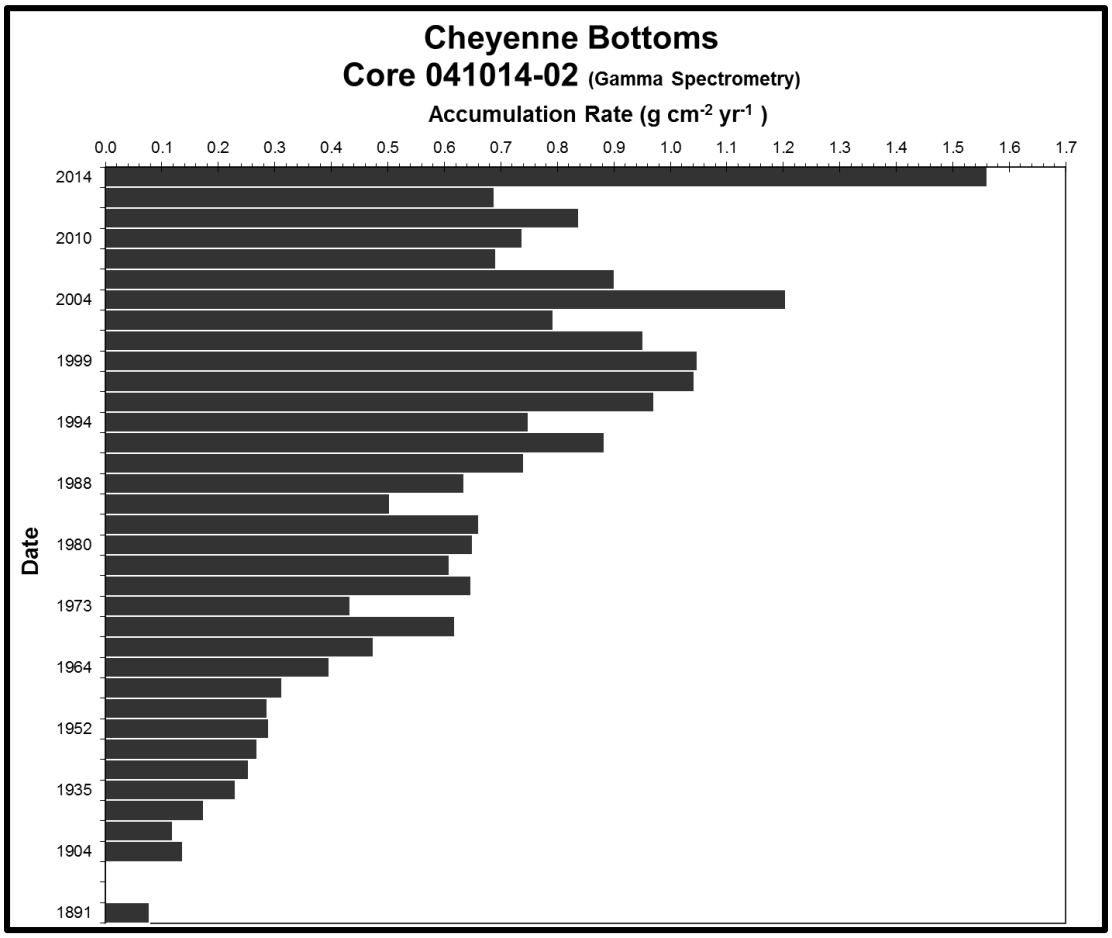

Figure 18: Sediment accumulation rate vs time for the Cheyenne Bottoms core, based on ^{210}Pb analysis.

The Cs peak in the Cheyenne Bottoms core occurs at 7.7 cm downcore (Figure 20). This date does not agree with the ^{210}Pb analysis, which places 1963 at ~25 cm downcore (Figures 18 and

19). The ^{210}Pb data were assumed to be more reliable than the ^{137}Cs data, due to the greater potential mobility of Cs in the sediment column (Stanners and Aston, 1981; Olsen, et al., 1982; Kirchner and Ehlers, 1998; Walker, 2005). Therefore, the lead-210 results were used for constructing a core chronology for Cheyenne Bottoms.

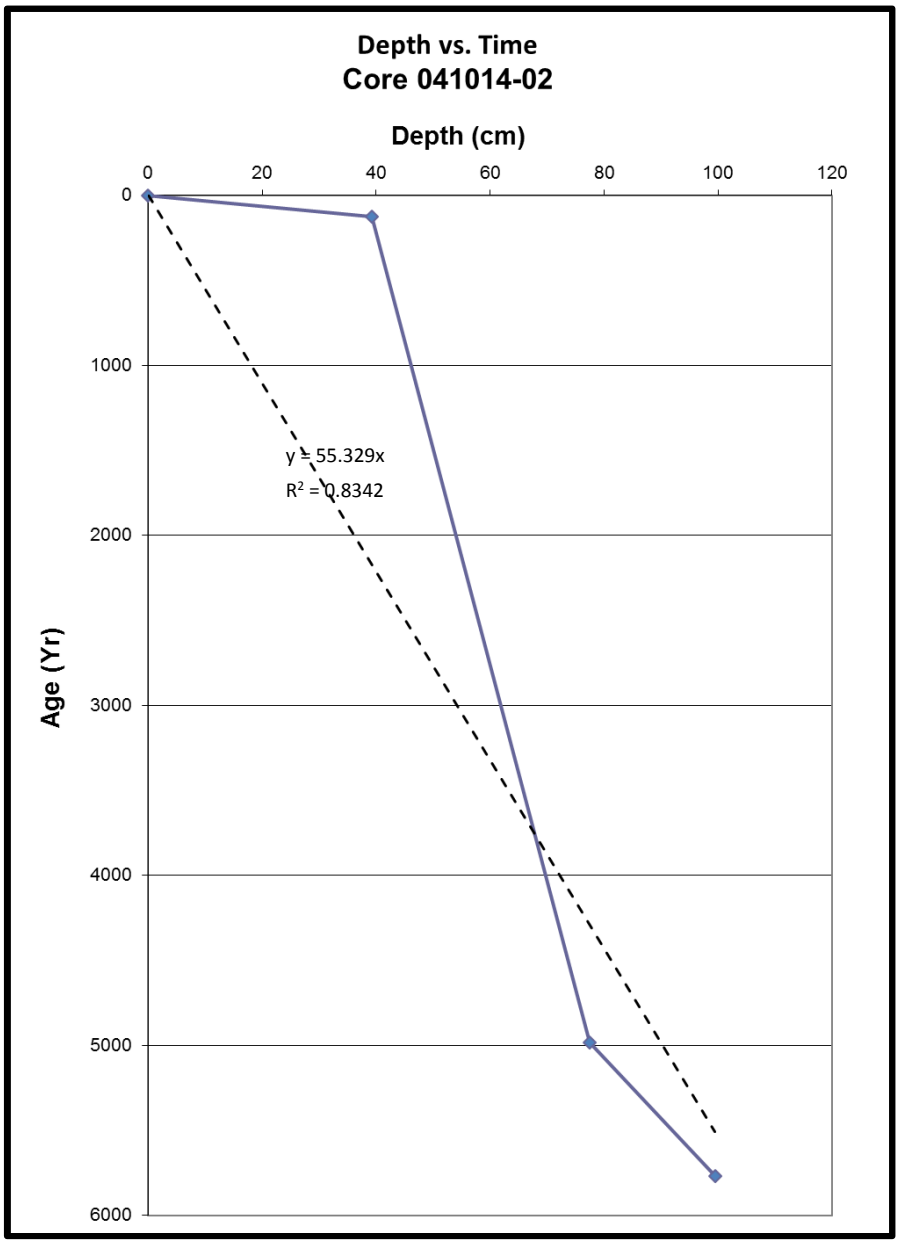

Figure 19: Age-Depth relationship for core 041014-02 from Cheyenne Bottoms, Kansas. Dashed line is a linear regression. Ages were calculated using slopes of the individual line segments lines.

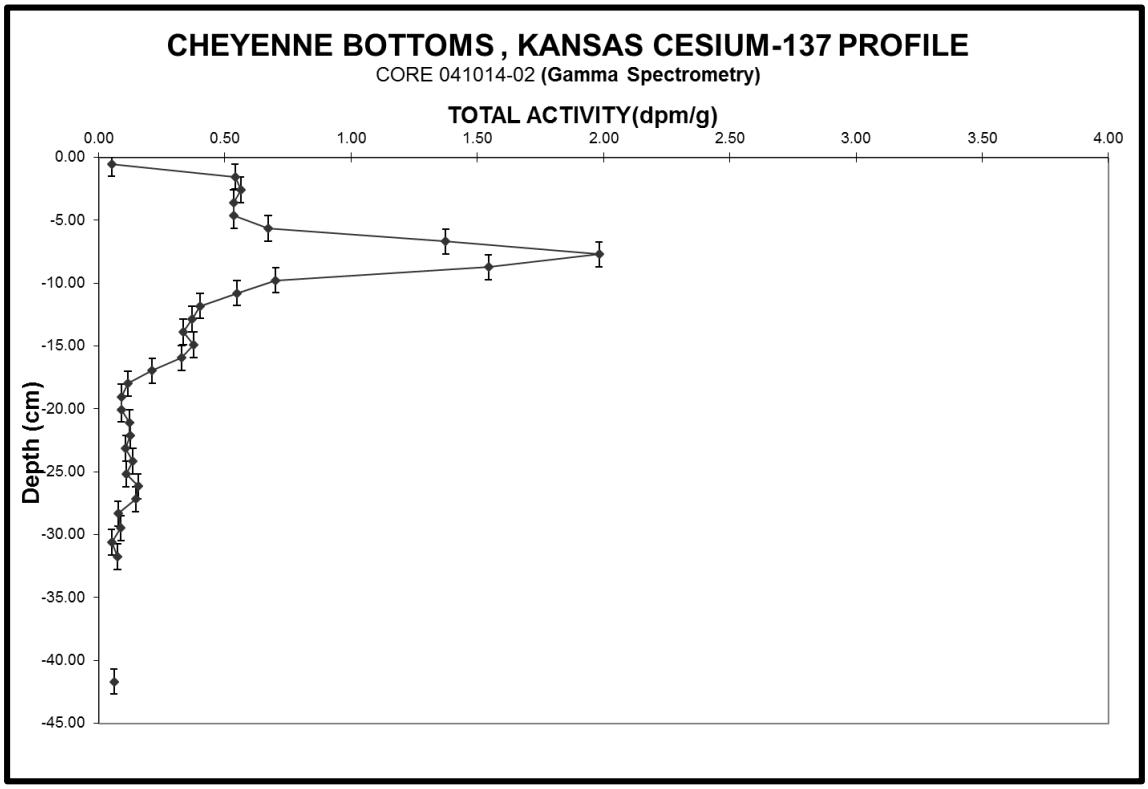

Figure 20: ^{137}Cs profile obtained from gamma spectrometry analysis. The 1963 peak in cesium activity is at 7.7 cm while the earliest appearance of the isotope occurs around 18 cm.

3.2.2 Canton Lake

The initial project plan was to use the Canton Lake core to establish the signature of major storms impacting a lake. An EF-3 tornado passed over the lake on May 24, 1011, as discussed above. The goal was to use a ^{210}Pb chronology of the core in order to fix the depth of the 2011 storm, and then to use the sedimentary parameters of that horizon in order to define the signature of storms in lake sediments. The Canton Lake samples were analyzed using the identical procedure that produced the Cheyenne Bottoms gamma data. However, gamma spectrometry resulted in a profile of background ^{210}Pb, but no excess (fallout) ^{210}Pb and no detectable fallout ^{137}Cs.

One possibility for the absence of decay profiles of ^{210}Pb and ^{137}Cs is that the sediment are deficient in clay particles, which provide the primary adsorption sites for trace metals, and that little or no Pb and Cs were adsorbed. Another possibility is that the core sediment was all deposited at one time in a large-scale sedimentation event. The latter possibility seems less likely, due to the heterogeneous nature of the sediment profile (Fig. 16).

In the absence of an absolute core chronology, a reasonable assumption can be made that the entire core profile is younger than the age of the dam that formed the lake (66 years). Therefore, the sediment analyses of the core can be assumed to reflect an approximately six-decade history of storms impacting the lake. A reasonable assumption is that the large excursion in the data at ~50 mm depth (Fig. 16) represents the 2011 storm, and that all or most of the overlying sediment were deposited during that event. Similar excursions downcore (+1 standard deviation in percent sand; -1 standard deviation in mean phi diameter) can then be taken to represent storm events. There are five, and perhaps six, such horizons in the core profiles.

CHAPTER IV

DISCUSSION

4.1 Determination of a Paleostorm Signature

After analyzing the textural data in the sediment cores and comparing these data with the historic record of recent storms, the geologic signature of midcontinent storms was identified. The storm signature was determined to be shifts, usually greater than 1 standard deviation of the mean difference, in both percent sand (+1 standard deviation) and mean grain size (-1 standard deviation). As in a recent study by Coor (2012), depending on the sedimentation rate, the positive peaks may be representative of a single storm event, or of periods during which one or more storms occurred.

Due to the unresolved core chronology for Canton Lake, the known storm event cannot be identified with complete confidence. It seems most likely that the large shift in mean grain size and percent sand at 50 mm is the May 2011 storm (Figure 16). This is in agreement with the results from the Cheyenne Bottoms core.

Within the proximity of Cheyenne Bottoms there have been 14 recorded storms since 1950 (NOAA/NWS, 2014) (Table 3). The Enhanced Fujita Scale, or EF Scale, is used to assign a tornado a 'rating' based on estimated wind speeds and related damage. When tornado-related damage is surveyed, it is compared to a list of Damage Indicators (DIs) and Degrees of Damage (DoD) which help

better estimate the range of wind speeds the tornado likely produced. From that, a rating (from EF0 to EF5) is assigned. A good correlation is found when the known storm events were compared with the mean grain size and percent sand differences (Figure 21) (Table 4). Differences in percent sand align better with the larger storms as shown in Figure 16 and Table 4. Storms greatly increase the energy in the system and consequently increase the ability to move larger sediment particles. This could be the cause of the large shifts in percent sand, usually greater than + 1 standard deviation, which correlated well with known storm events. Since the sedimentation rate for upper part of the core, 0 - 40 cm, averages about 0.3 cm/yr, the shifts in percent sand and mean grain size represent times of greater or lesser storminess, and do not necessarily resolve individual storm events. While a large storm event may have occurred during the multi-year span, it is impossible to say that it was the only storm which affected the system. The larger storms in particular match well with the shifts in percent sand. These storms are mostly EF-3 or greater and occur at depths of 7.6 cm, 12.3 cm, and 18.3 cm, based on the ^{210}Pb chronology (Table 4). It is possible that more violent storms have a greater effect on the system by inputting a much larger quantity of sand-sized particles. However, smaller storms, < EF-3, are also identifiable on the sediment profiles (Figure 21 and Table 4). For weaker storms to influence the sedimentology of the system, the storm most likely needs to be much closer to the sample site due to its smaller path radius and lower wind speeds.

Table 3: Date and magnitude, on the Enhanced Fujita scale, of tornadoes which have passed within a 10 km radius of the core location at Cheyenne Bottoms, Kansas (NOAA/SPC, 2014).

Date	Magnitude
April 2, 1956	3
May 27, 1975	3
May 24, 1990	3
July 4, 1993	0
May 10, 1999	1
April 1, 2001	4
May 11, 2002	0
March 27, 2004	0
April 19, 2005	0
April 19, 2005	1
May 5, 2007	1
June 12, 2010	0
May 24, 2011	0
May 24, 2011	1

Table 4: Depths and ages for all peaks in both the percent sand difference and mean grain size difference profiles. Ages are in years before the sampling date, based on ^{210}Pb chronology. Also shown are depths and ages for known historical storms within an approximate 10 km radius of Cheyenne Bottoms and magnitude on the Enhanced Fujita scale. Storm data from NOAA\SPC (2015).

Peaks in Percent Sand		Peaks in Mean Grain Size		Historical Storms		
Depth	Age	Depth	Age	Depth	Age	Magnitude
(cm)	(yr)	(cm)	(yr)	(cm)	(yr)	(EF)
0.5	2	2.9	9	0.9	3	1
0.9	3	8.4	27	0.9	3	0
2.9	9	9.4	30	1.3	4	0
4.3	14	24.1	76	2.2	7	1
8.7	28	28.6	90	2.8	9	1
9.4	30	53.4	1926	2.8	9	0
12.1	38	72.2	4311	3.2	10	0
14.2	45	73.3	4450	3.8	12	0
15.2	48	79.0	5037	4.1	13	4
19.0	60	87.7	5348	4.7	15	1
20.7	65	89.9	5426	6.6	21	0
23.8	75	99.0	5752	7.6	24	3
29.2	92			12.3	39	3
35.4	112			18.3	58	3
42.9	136					
45.3	898					
47.6	1190					
51.1	1634					
52.8	1850					
65.9	3512					
73.4	4463					
75.6	4742					
76.8	4894					

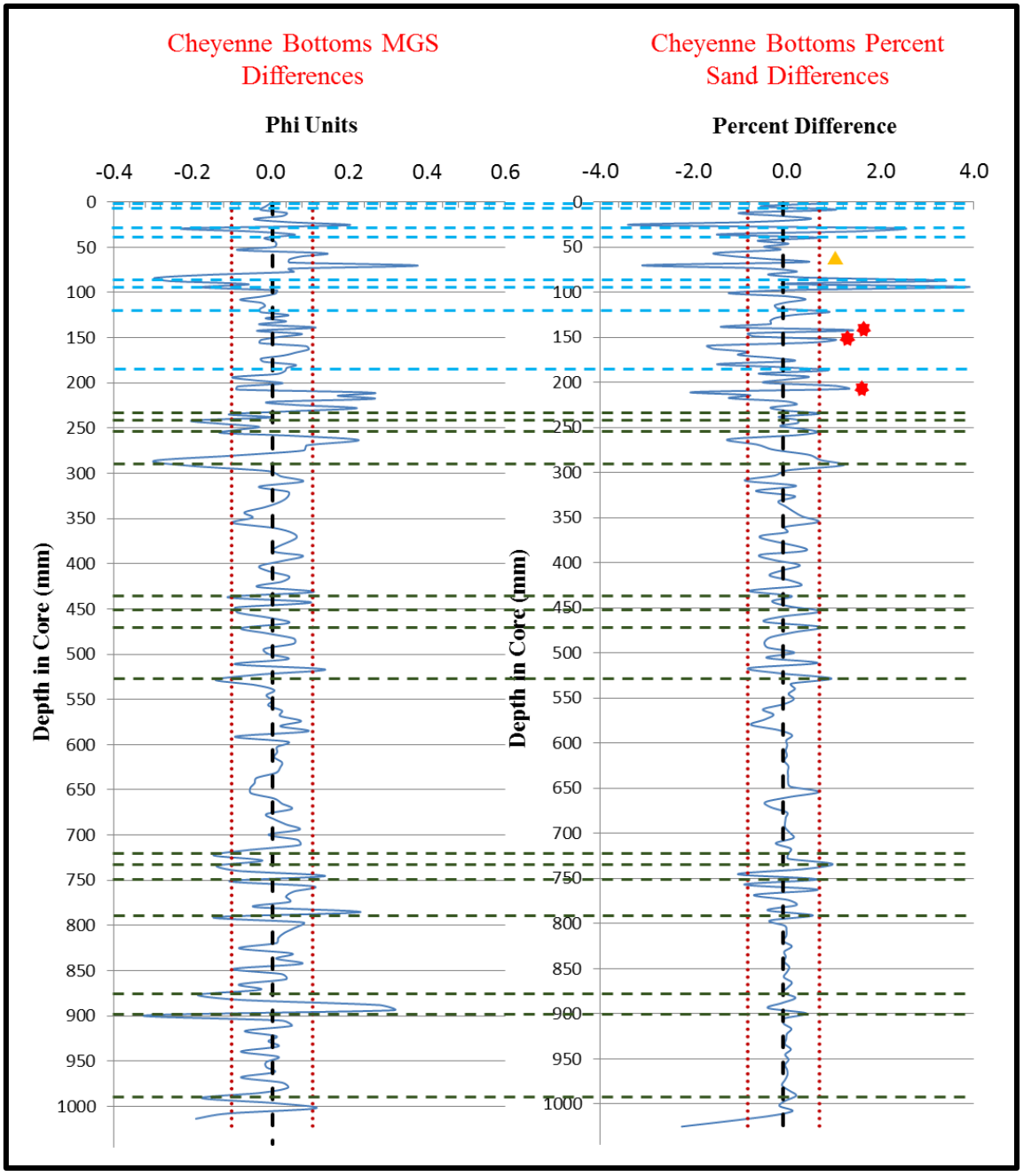

Figure 21: Downcore differences in percent sand and mean grain size. Storm events were chosen based on large positive shifts in percent sand and/or corresponding negative shifts in phi size. Light blue dashed lines represent known historic storm occurrences, based on ^{210}Pb chronology. Green dashed lines represent possible extreme events in the prehistoric storm record. Red stars are false positives and orange triangles are false negatives.

There are some inconsistencies in the data that can be interpreted as either false positive or false negatives on the sediment profiles as seen in Figure 21. There are three potential false positives and one false negative. False positives may represent events other than storms that alter the environmental energy enough to change the sedimentologic profile. Since 1885, Cheyenne Bottoms, Kansas has experienced nine major flooding events (Zimmerman, 1990). Such floods and other events can create false positives in the sediment profiles. The false positives were identified by having a large shift in percent sand differences with only a minor negative shift in phi units. Storm events in the historic record typically display large negative shifts in phi units with equivalent peaks in percent sand difference (Figure 21). False negatives represent known storms that do not show up as peaks greater than + 1 standard deviation on the percent sand profiles. These storms may have occurred too far away to affect sediment in the lake, or the wind speed needed to lift larger grains might not have been strong enough to change the sedimentology sufficiently to alter the core profile. Moreover, the sampling interval might have not been high resolution enough to capture smaller periods of greater or lesser storminess and thus smaller changes, and consequently certain storms could be missed during analysis.

After detailed analysis of the historic storm data and the Cheyenne Bottoms core sediment texture data, it is possible to say that individual storms can significantly alter the mean grain size and sand percentage in the lake sediments. Positive shifts in primarily the downcore differences in percent sand seem to be the primary sedimentologic signature created by large storms in the past. In the long-term record it is, however, not possible to discern individual events due to compaction and slower sedimentation rates. Nonetheless, it is possible to discern periods during which major storms occurred and thus make inferences about changes in storm frequency through time (Figure 21).

Analysis of storm events was examined using the particle size distribution plot (PSD) created using Geosoft Oasis Montaj (Figure 22). The PSD plot allows for the identification of

subtle changes and trends in the sediment record which might not be easily identified in the normal sediment profiles (Figures 15 and 16). There is a good correlation between the standard core profiles and the PSD plot. The chief benefit of the PSD plot is that it provides useful information on the sediment grain size category (fine sand) that is most affected by the postulated storm events.

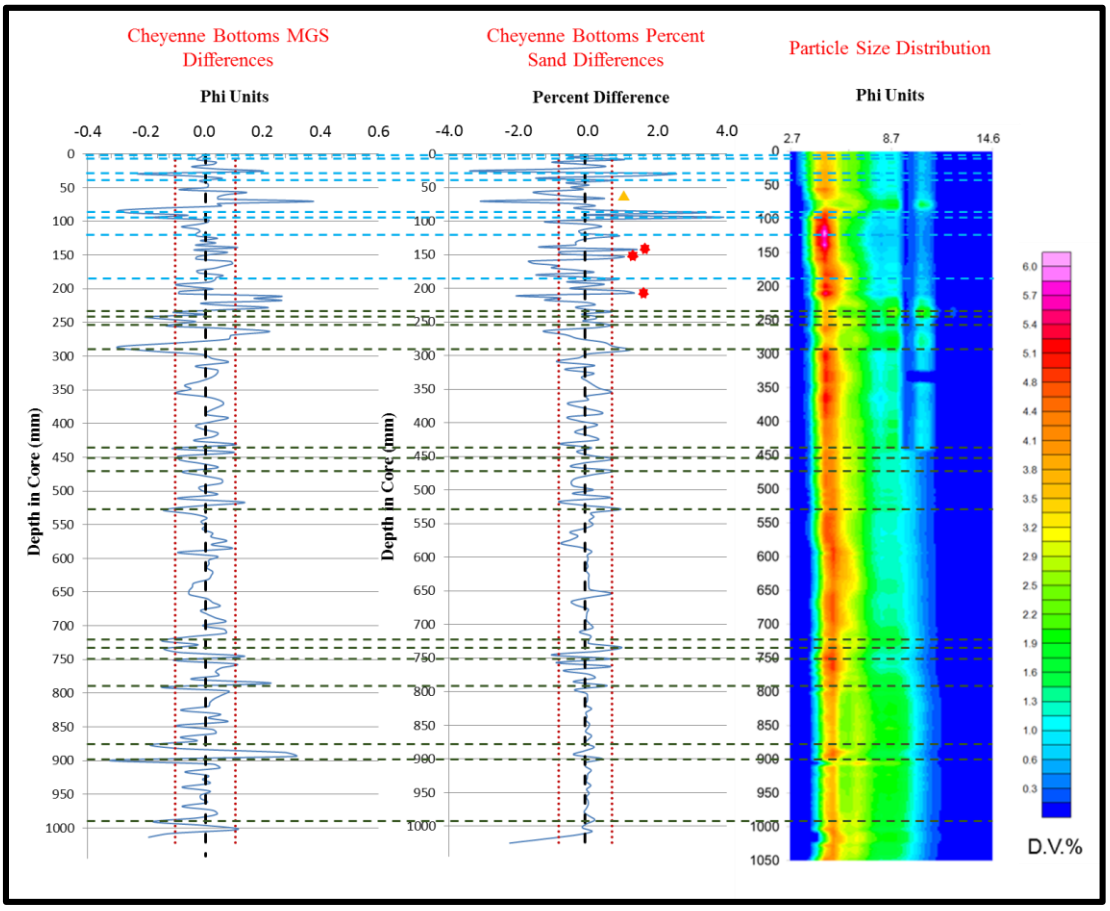

Figure 22: Textural parameter profiles compared with particle-size distribution (PSD) plot. Light blue lines represent known historic storm occurrences, based on ^{210}Pb chronology. Green lines represent possible extreme events in the prehistoric storm record. Red stars are false positives and orange triangles are false negatives. Red dotted lines represent known and potential storm events. Scale for PSD plot, at right, represents differential volume (DV) percent for each sediment grain size class. Grain sizes on PSD plot range from coarse (2.7 phi, fine sand) at left to fine (14.6 phi, clay size) at right. PSD plot from Lutiker et al. (2015).

The Canton Lake sediment data were analyzed in the same manner as the Cheyenne Bottoms core data. Since 1950, nine storms have occurred in the Canton Lake region and should have affected the sedimentology of the system (NOAA/SPC, 2015) (Table 5). As above, storms were chosen based on shifts, usually greater than 1 standard deviation of the mean difference, in both percent sand (+1 standard deviation) and mean grain size (-1 standard deviation). Using those criteria storms, false positives, and false negatives were identified for the Canton Lake core (Figure 23).

Table 5: Date and magnitude, on the Enhanced Fujita scale, of tornadoes which have passed within a close proximity of the core location at Canton Lake, OK (NOAA/SPC, 2014).

Date	Magnitude
June 5, 1953	1
July 22, 1956	0
May 26, 1963	1
May 13, 1965	1
April 11, 1966	1
April 20, 1984	1
June 13, 1998	0
September 21, 1998	0
May 24, 2011	3

Table 6: Depths and ages for all peaks in both the percent sand difference and the mean grain size difference profiles. Ages are in years before the sampling date. Also shown are depths and ages for known historical storms within close proximity to Canton Lake, OK. Storm data from NOAA\SPC (2015)

Peaks in Percent Sand	Historical Storms		
Depth	Age	Magnitude	Depth
(cm)	(yr)	(EF)	(cm)
2.3	3	3	4.9
5.0	16	0	19.4
8.1	16	0	19.4
10.7	30	1	34.9
11.6	48	1	54.9
17.6	49	1	56
22.2	51	1	58.2
34.1	58	0	66
37.0	61	0	69.3
45.5			
61.2			
65.4			
68.6			

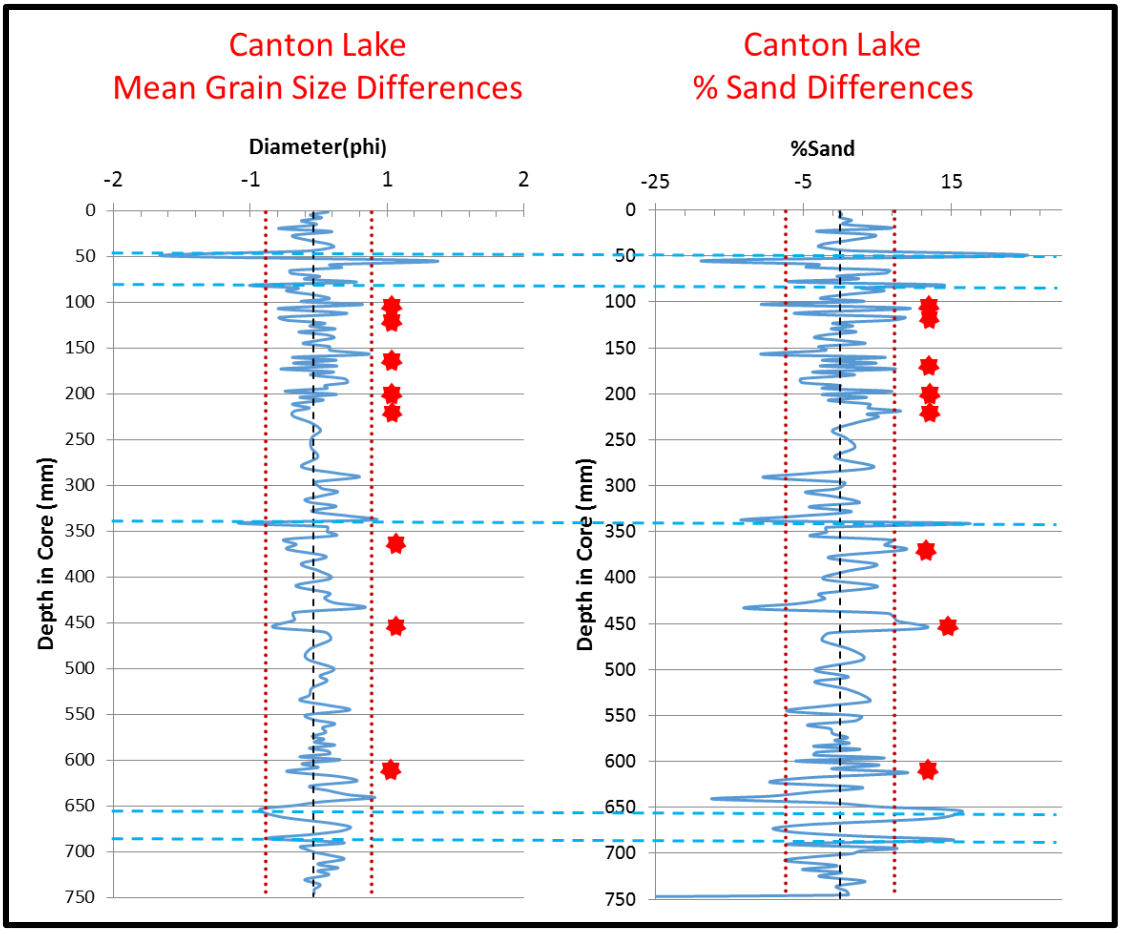

Figure 23: Downcore differences in percent sand and mean grain size. Storm events were chosen based on large positive shifts in percent sand and corresponding negative shifts in phi size. Light blue lines represent known historic storm occurrences. Red stars are false positives and orange triangles are false negatives.

4.2 Paleostorm Frequency

In order to create a paleostorm frequency model there must be guidelines for choosing storms that are able to influence the sediment textural parameters of a certain location. For this study, storms that would have been able to impact Cheyenne Bottoms sedimentologically were first examined based on the study by Elsner et al. (2014). According to Elsner et al. (2014), as the magnitude of a storm increases, the structural damage path width increases (see Figure 24). The results of the study can be used to define a minimum radius of influence within which a tornado

could impact sediment input for a certain location. Using data from Elsner et al. (2014) and the NOAA/SPC tornado database, storms that occurred close to Cheyenne Bottoms might be included or excluded from the paleostorm frequency model based on their magnitude and proximity to the site.

Storm locations and their paths were plotted on Google Earth using data from the NOAA/SPC database. However, as shown in Figure 24, the damage path radii for each corresponding EF magnitude, centered on the core location at Cheyenne Bottoms, do not encompass any storms, large or small. It can be speculated that the Elsner et al. (2014) structural damage radii are not necessarily equal to the radii of sediment influence for a given area. Elsner et al. (2014) use the definition of damage provided under the EF-Scale guidelines as shown in Table 7. A certain DOD, or degree of damage, can include a large variation in wind speed and damage path width. Moreover, the wind speeds created by storms are much larger than the minimum wind speeds needed to initiate grain movement, as illustrated in Figure 25. In Figure 24, the fluid threshold velocity is the minimum wind speed necessary to initiate grain movement by the force of wind alone. The wind speeds needed to move grains in the diameter range observed at Cheyenne Bottoms are only 25 – 40 cm/s. Therefore, it can be concluded that tornadoes' influence on the sediment texture of an area is much larger than the structural damage path radius established by Elsner et al. (2014). A proposed radius of ~ 10 km (Figure 24) would include 14 historic tornadoes as shown in the figure.

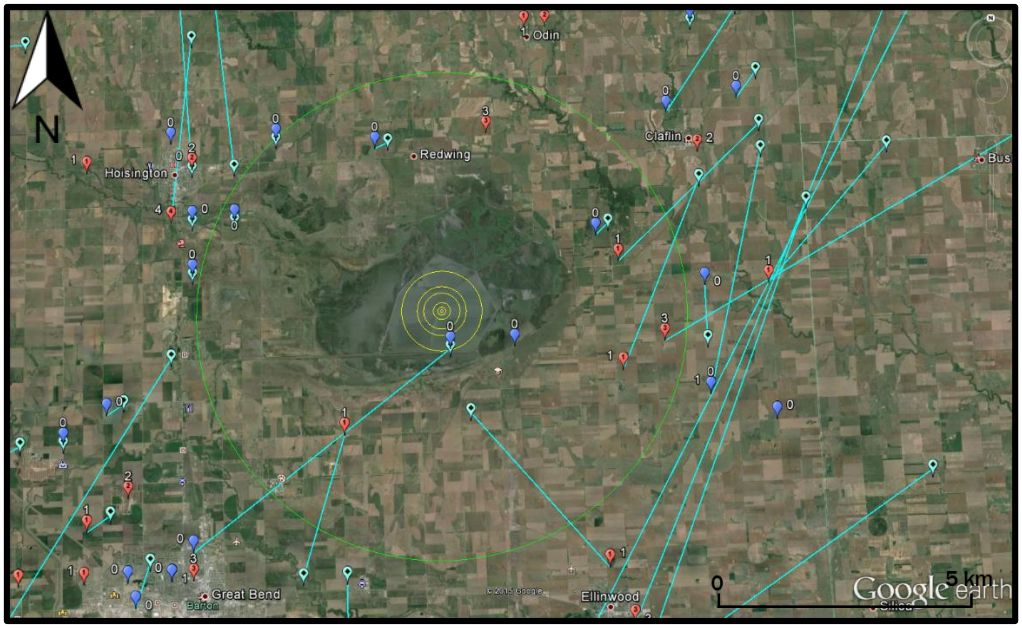

Figure 24: Cheyenne Bottom wildlife refuge, showing the magnitudes of storms since 1950 with their corresponding paths if known. The yellow concentric circles (55m, 164m, 344m, 736m, 998m, and 1635m) show the damage path radii based on Elsner, et al. (2014). The green circle shows a proposed radius of 10,000 meters for sediment influence at the core location.

Table 7: Degree of damage with corresponding wind speeds (Exp – Expected; LB – Lower Bound; UB – Upper Bound), EF-Scale Rating, and damage path radii (Elsner et al., 2014). Expected wind speed is the average wind speed needed to produce the corresponding degree of damage. The EF scale is interpreted based on the observed DoD created from a tornado. Modified from NOAA/SPC, 2015.

DOD*	Damage Description	EXP	LB	UB	Corresponding EF-Scale Rating	Damage Width (m)
1	Threshold of Visible Damage	65	53	80	EF-0	54.9
2	Loss of roof covering material (<20%), gutters and/or awning; loss of vinyl or metal siding	79	63	97	EF-0, EF-1	54.9 - 163.8
3	Broken glas in doors and windows	96	79	114	EF-0, EF-1, EF-2	54.9 - 344.1
4	Uplift of roof deck and loss of significant roof covering material (>20%); collapse of chimney; garage doors collapse inward or outward; failure of porch or carport	97	81	116	EF-0, EF-1, EF-2	54.9 - 344.1
5	Entire house shifts off foundation	121	103	141	EF-1, EF-2, EF-3	163.8 - 736.3
6	Large sections of roof structure removed; most walls remain standing	122	104	142	EF-1, EF-2, EF-3	163.8 - 736.3
7	Top floor exterior walls collapse	132	113	153	EF-2, EF-3	344.1 - 736.3
8	Most interior walls of top story collapse	148	128	173	EF-2,EF-3,EF-4	344.1 - 997.9
9	Most walls collapsed in bottom floor, except small interior rooms	152	127	178	EF-2,EF-3,EF-4	344.1 - 997.9
10	Total destruction of entire building	170	142	198	EF-3,EF-4	736.3 - 997.9
	*Degree of Damage					

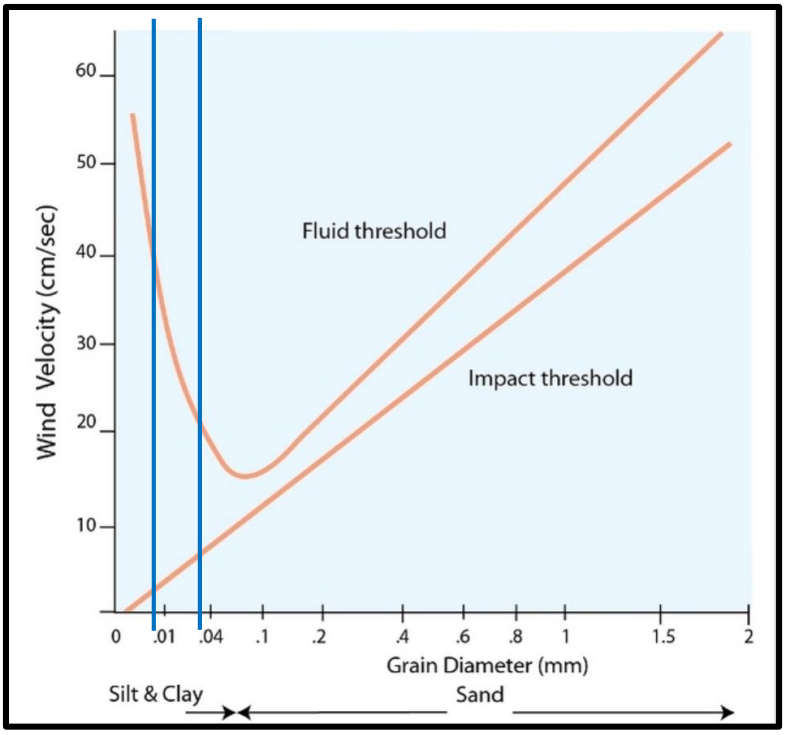

Figure 25: Relationship between grain diameter and wind velocity. The fluid threshold velocity is the minimum wind speed necessary to initiate grain movement by the force of wind alone. The impact threshold is the minimum wind speed needed to initiate particle movement as a result of grain impact. Size range for Cheyenne Bottoms sediment lies within the blue lines (Bettis, 2012).

4.3 Climate Change

A proxy climate record for Cheyenne Bottoms and the nearby Great Plains region has been established previously, based on pollen data (Fredlund, 1992; Baker and Waln, 1985; Fredlund and Jaumann, 1987; Sadeghipour and McClain, 1987). The pollen record was compared with the record of paleostorm occurrence developed during this investigation.

The late Quaternary climate history of Cheyenne Bottoms was described by Fredlund, (1992). The four major climate periods (Farmdalian, Woodfordian, Woodfordian – Holocene Transition, and Holocene) were examined for trends, using sediment and pollen analysis. According to Fredlund (1992), between 30,000 and 24,000 yr. BP, a grassland – sage steppe

dominated the regional uplands surrounding the basin, from 25,000 to 24,000 yr. BP there was a basin-wide drying cycle. The Woodfordian climate varied from cold xeric conditions from 24,000 to 16,000 yrs. BP to cooler and more mesic conditions from 16,000 to 12,000 yrs. BP (Fredlund, 1992).

The Holocene pollen assemblages are dominated by "Cheno-Am" type pollen, which are part of the grasses family, and in this instance are probably derived from local mudflat communities (Fredlund, 1995). This Cheno-Am mudflat community is an early successional stage rapidly replaced by grasses and forbs if not frequently flooded and exposed (Fredlund, 1995). The mid-Holocene (ca 8,500 to 3,700 yr BP) shows a large decrease in Cheno-Am percentages, which is said to represent an increase in aridity and is most likely a function of more stable and possibly lower water levels in the lake (Fredlund, 1995). From 3700 yr BP to present, a rise in Cheno-Am pollen percentages was interpreted to indicate an increase in water level fluctuations and exposure of mudflats (Fredlund, 1995). Rises in Cheno-Am percentages are a result of greater fluctuation in the water level, allowed for larger areas to be open to colonization. Stability in the basin's water budget at any level, should reduce the area of exposed mudflats and therefore create opportunity for the Cheno-Am invasion (Fredlund, 1995).

Fredlund's (1995) climate record was compared to the paleostorm model of this study. According to Fredlund, the mid-Holocene, 8,500 to 3,700 yr BP, had warmer temperatures and less precipitation, compared with the early and late Holocene. It is difficult to make judgments on the storm frequency during that time when the estimated oldest age of the core is approximately 6,000 years. The late Holocene transition occurs at approximately 64 cm downcore. Moving up core there are many fluctuations in periods of greater or lesser storminess.

4.4 Return Periods

Return periods were calculated for storms larger than EF-3 on the Fujita scale using the historic and pre-historic paleostorm frequency and intensity data.

For the historic record from 1950 - 2013, return periods for large storms were calculated using the NOAA/SPC database. Since 1950 there have been 4 storms greater than EF-3 within a 10 km radius of Cheyenne Bottoms Wildlife Refuge (NOAA/SPC, 2014). The return period for the Cheyenne Bottoms region is approximately 16 years for storms > EF- 3, calculated using the historic record provided by NOAA/SPC database.

In the prehistoric record, due to the constraints of the sampling interval, we cannot identify individual storms. We can, however, detect periods of greater or lesser storminess. Storm frequency in the prehistoric record shows periods of both increased and decreased storminess (Figure 26). An arbitrary period of 200 years was used, in order to encompass a sufficient number of samples, in this case three to five. In Figure 26, the minimum number of storms per 200-year segment is shown versus age in years. There are five distinct periods when at least one significant storm event occurred. It should be emphasized that this represents the minimum number of storms during that period. These periods represent times in the prehistoric record where there was increased storm activity.

Several sites in the northern Great Plains have contributed proxy evidence of a climatic change from a more arid mid-Holocene (low effective moisture) prior to about 4500 years ago to one of increasing effective moisture, which continued until about 2000 years ago (Laird et al., 1996; radiocarbon dates corrected to calendar dates using CALIB 7.1. The arid period prior to about 4500 years ago occurs during a time of increased storminess represented in our paleostorm model. The shift to a period of increasing effective moisture correlates well with our paleostorm model. We see low storm activity during periods of a cooler climate. The Medieval Warm Period

(approx. 900 to 700 years ago) is represented by an increase in storm activity from about 1000 to 700 years ago on the paleostorm model (Laird et al., 1996). The Little Ice Age (about 500 to 100 years ago) is represented by the decrease in storm activity beginning about 700 years ago. There appears to be a relationship between climate and prehistoric storm frequency. Periods of increased aridity or increased temperatures correlate well with times of increased storminess from the paleostorm model. It is possible that rising temperatures also result in a rising storm frequency.

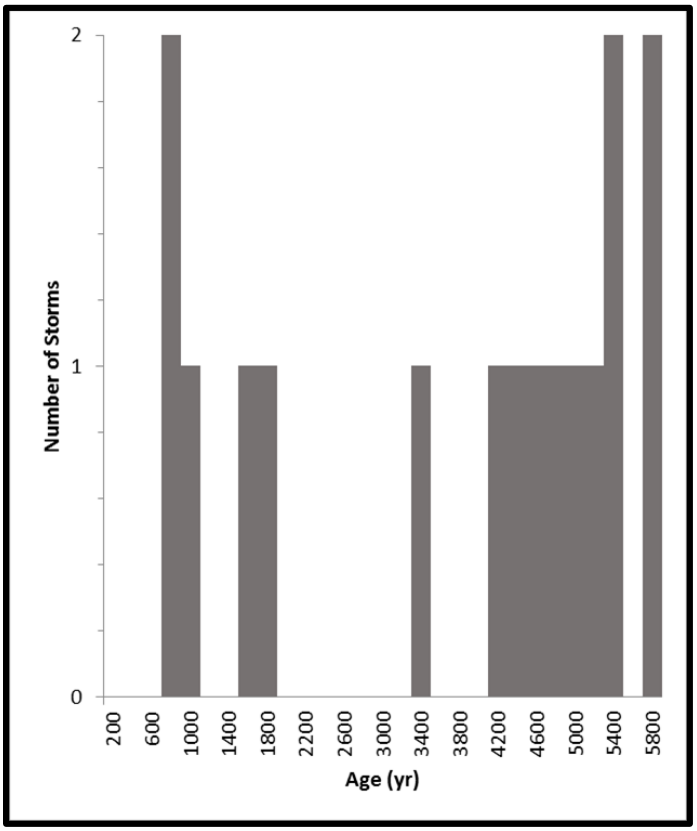

Figure 26: Major storm history for Cheyenne Bottoms, KS, based on the paleostorm model. The minimum value for storm occurrence per 200-year period is show for the past six millennia. There are five periods of increased activity separated by periods of low activity. Periods of activity were represented by a minimum of one storm per 200 years.

CHAPTER V

CONCLUSION

Return periods for large historic storms (>EF-3) were calculated using the NOAA/SPC storm database. In the prehistoric record return periods were not capable of being calculated because the sedimentation rates were too slow and individual storms could not be identified. Nonetheless, fluctuations in storm frequency were still identified and can give implications into the variations in climate during that period. The paleostorm model constructed was compared with other climate proxies in the Great Plains region. The periods of greater storminess correlate well with periods of increased aridity or higher temperatures. Therefore, the paleostorm model can be used to better understand local climate regimes and their fluctuations with changing climate.

With the establishment of a proxy for identifying storm events or periods of storminess in the sedimentological record of lakes or wetlands, more detailed analysis of changes in storm frequency with climate or temperature can be analyzed. This study creates the potential for a more long-term analysis of storm trends and therefore better prediction capability into the future.

REFERENCES

Baker, R.G., and Waln, K. A. 1985. Pollen records from the Great Plains and central United States, Chapter 8, In Pollen Records of Late-Quaternary North American Sediments (Bryant, V.M. Jr., and Holloway, R.G., Eds.) The American Association of Stratigraphic Palynologists Foundation, p.191-203

Balsillie, J. H., Donoghue, J.F., Butler, K.M., Koch, J.L., 2002. Plotting equation for Gaussian percentiles and a spreadsheet program for generating probability plots. Journal of Sedimentary Research 72, 929-933.

Bayne, C. K., 1977, Geology and structure of Cheyenne Bottoms, Barton County, Kansas. Geological Survey of Kansas Bulletin, 211, 1-12.

Berz, G.A. 1993, Global warming and the insurance industry. Interdisciplinary Science Review, 18,120-125.

Bettis III, A. E. 2012. Climatic and biotic controls on silt production and accumulation of loess. Nature Education Knowledge 3(10):25

Boose, E. R., Chamberlin, K.E., Foster, D.R., 2001. Landscape and regional impacts of hurricanes in New England. Ecological Monographs 71, 27-48.

Botter-Jensen, L. 1997. Luminescence techniques: Instrumentation and methods. Radiation Measurements, 27, 749-768.

Brooks, H. E., Lee, J.W., Craven, J.P., 2003. The spatial distribution of severe thunderstorm and tornado environments from global reanalysis data. Atmos. Res., 67-68, 73–94.

Brooks, H. E., Dozek, N., 2008. The spatial distribution of severe convective storms and an analysis of their secular changes, in Climate Extremes and Society, edited by H. F. Diaz and R. Murnane, pp. 35–54, Cambridge Univ. Press, New York.

CALIB 7.1, (Stuiver, M., Reimer, P., and Reimer, R.)http://calib.qub.ac.uk/calib/calib.html (accessed 04/01/2015).

Chanton, J.P., Martens, J.S., Kipphut, G.W., 1983. Lead-210 sediment geochronology in a changing coastal environment. Geochimica et Cosmochimica Acta 47, 1791-1804.

Changnon, S.A., Changnon, J.M., 1992. Temporal fluctuations in weather disasters: 1950-1989. Climatic Change, 22,191-208.

Cook, A. R., Schaefer, J.T., 2008. The relation of El Niño– Southern Oscillation (ENSO) to winter tornado outbreaks, Mon. Weather Rev., 136, 3121–3137.

Coor, J.L., 2012. Coastal Lake Paleoclimate Records: Late Quaternary Paleostorm Chronology for the Northeastern Gulf of Mexico Coast. Unpubl. PhD Dissertation, Florida State University, 114 p.

Das, O., Wang, Y., Donoghue, J.F., Xu,X., Coor, J.L., Elsner, J., and Xu, Y., 2013, Reconstruction of paleostorms and paleoenvironments using geochemical proxies archived in sediments of two coastal lakes in northwest Florida: Quaternary Science Reviews, v. 68, p. 142-153.

Del Genio, A. D., M. S. Yao, and J. Jonas, 2007, Will moist convection be stronger in a warmer climate? Geophys. Res. Lett., 34, L16703, doi: 10.1029/2007GL030525.

Diffenbaugh NS, Trapp RJ, Brooks H., 2008. Does global warming influence tornado activity. EOS Trans, Am Geophys Union 89(53):553–560

Duke, W.L., 1984. Paleohydraulic analysis of hummocky cross-stratified sands indicated equivalence with wave-formed flat beds: Pleistocene Lake Bonneville deposits, northern Utah. Bull. Am. Assoc. Petrol. Geol. 68, 472.

Duke, W.L., 1985. The paleogeography of paleozoic and mesozoic storm depositional systems: A discussion. Journal of Geology, 93 (1) 88-90.

Elsner, J.B., Lewers, S.W., Malmstadt, J.C., Jagger, T.H., 2011. Estimating contemporary and future wind-damage losses from hurricanes affecting Elgin Air Force Base, Florida. Journal of Applied Meteorology and Climatology 50, 1514-1526.

Elsner, J.B., Murnane, R.J., Jagger, T.H., Widen, H.M. 2013. A Spatial Point Process Model for Violent Tornado Occurrence in the US Great Plains. Math Geosci (2013) 45:667–679

Elsner JB, Jagger TH, Elsner IJ (2014) Tornado Intensity Estimated from Damage Path Dimensions. PLoS ONE 9(9): e107571. doi:10.1371/journal.pone. 0107571

Emanuel, K. A., 1995, Sensitivity of tropical cyclones to surface exchange coefficients and a revised steady-state model incorporating eye dynamics. Journal of Atmospheric Science 52, 3969 – 3976.

Emanuel, K.A., 2005. Increasing destructiveness of tropical cyclones over the past 30 years. Nature 436, 686-688.

Etkin, D.A., 1995. Beyond the year 2000, more tornadoes in western Canada, implications from the historical record. Nat Hazards.12:19-27.

Folk, R. L., 1974. Petrology of Sedimentary Rocks: Austin, TX, Hemphill Publ., 182 p.

Fredlund, G.G., and Jaumann, P.J., 1987. Late Quaternary palynological and paleobotanical records from the central Great Plains. Kansas Geological Survey Guidebook Series 5. Pp 167-178.

Fredlund, G. G., 1992. "Analysis of Quaternary Pollen from Cheyenne Bottoms, Kansas: Evidence for Late Quaternary Vegetation and Climates in the Central Great Plains." Unpublished Ph.D. dissertation. University of Kansas, Lawrence. Pp 1-186.

Fredlund, G.G., 1995. "Late quaternary pollen record from Cheyenne Bottoms, Kansas." Quaternanry Research 43, 67-79.

Friedman, D.G., 1988. Implications of climate change for the insurance industry. Proceedings of the North American Conference on Preparing for Climate Change. Climate Institute, Washington, DC. 389-400.

Grazulis, T.P., 1993. A 110-year perspective of significant tornadoes. In: Church C, Burgess D, Doswell C, Davies-Jones R, editors. The tornado: its structure, dynamics, prediction, and hazards. American Geophysical Union Geophysical Monograph 79:467-474.

Harms, J. C.; Southard, J. B.; Spearing, D. R.; and Walker, R. G., 1975. Depositional environments as interpreted from primary sedimentary structures and stratification sequences: Soc. Econ. Paleont. Mineral. Short Course No. 2, 161

Hassan, K.M., Swinehart, J.B., Spalding, R.F., 1997. Evidence for Holocene environmental change from C/N ratios, and d13C and d15N values in Swan Lake sediments, western Sand Hills, Nebraska. Journal of Paleolimnology 18, 121-130.

Houghton, J. T., Jenkins, G. J., and Ephraums, J. J., 1990. *Climate Change: The IPCC Scientific Assessment*, Cambridge University Press, Cambridge, U.K., 365 pp.

Huntley, D.J., Godfrey-Smith, D.I. and Thewalt, M.L.W., 1985. Optical dating of sediments. Nature, 313, 105-107

Kirchner, G., Ehlers, H., 1998. Sediment geochronology in changing coastal environents: Potentials and limitations of the 137Cs and 210Pb methods. Journal of Coastal Research 14,483-492

Kim, K. H., and Burnett, W.C., 1983. γ-ray spectrometric determination of Uranium-series nuclides in marine phosphorites. Analytical Chemistry 55, 1796-1800

Krishnaswamy, S.,Lal, D.,Martin, J.M., Meybeck, M., 1971. Geochronology of lake sediments. Earth and Planetary Sciences Letters 11, 407-414.

Laird, K.R., Fritz, S.C., Grimm, E.C., Mueller, P.C., 1996. Century-scale paleoclimatic reconstruction from Moon Lake, a closed-basin lake in the northern Great Plains.Limnology Oceanography, 41, pp. 890–902

Lamb, A. L., Leng, M.J., Sloane, H.J., Telford, R.J., 2005. A comparison of the palaeoclimate signals from diatom oxygen isotope ratios and carbonate oxygen isotope ratios from a low latitude crater lake. Palaeogeography, Palaeoclimatology, Palaeoecology 223, 290-302.

Latta, B. F., 1950. Geology and ground-water resources of Barton and Stafford counties, Kansas: Kansas Geol. Survey Bull. 88, 228 p.

Leckie, D. A., and Walker, R. G., 1982. Storm-and tide-dominated shorelines in Cretaceous Moosebar-Lower Gates interval-outcrop equivalents of deep basin gas trap in western Canada: Am. Assoc. Petrol. Geol. Bull., 66, 138-157.

Liu, K.B., Fearn, M.L., 1993. Lake-sediment record of late Holocene hurricane activities from Coastal Alabama. Geology 21, 793-796.

Liu, K.B., Fearn, M.L., 2000. Reconstruction of prehistoric landfall frequencies of catastrophic hurricanes in northwestern Florida from lake sediment records. Quaternary Research 54, 238-245.

Long, J.A., Stoy, P.C., 2014. Peak tornado activity is occurring earlier in the heart of "Tornado Alley". Geophys. Res. Lett., 41, 6259-6264, doi: 10.1002/2014GL061385

Lutiker, Michelle A., McCollum, M.S., Donoghue, J.F., 2015, Development of a proxy for major storms in the midcontinent: Geological Society of America *Abstracts with Programs.* Vol. 47, No. 1, p.43

Marsh, P. T., et al. 2007. Assessment of the severe weather environment in North America simulated by a global climate model, Atmos. Sci. Lett., 8, 100–106.

McCollum, M.S., Donoghue, J.F., Lutiker, Michelle A., Sanders, Hannah, and McNabb, Tyler, 2015. Investigating the geologic record of paleo-storms from lake and wetland sediments of the Great Plains: Geological Society of America *Abstracts with Programs.* Vol. 47, No. 1, p.53

McNabb, T.S., 2014. Developing Proxies for Late Holocene Sea-Level and Climate Change along the Northeastern Gulf of Mexico Coast. Unpubl. Master's Thesis. Oklahoma State University, 79 p.

Milan, C.S., Swenson, E.M. Turner, R.E., Lee, J.M., 1995. Assessment of the 137Cs method for estimating sediment accumulation rates: Louisiana salt marshes. Journal Coastal Research 11, 296-307.

Morton, M.C., 2014. Twister season comes earlier to tornado alley. Earth Magazine, pp 14. (Accessed 03/25/2015)

Myrow, P.M., Southard, J.B., 1996. Tempestite Deposition. Unpubl. Report, Department of Geology, The College and Department of Earth, Atmospheric, and Planetary Sciences, Massachusetts Institute of Technology, pp 875-887.

Myrow, P. M. 1978. Storm deposits. In C.W., Finkl (Ed.), *Encyclopedia of Sedimentology* (Vol. 18, pp. 1139-1142). Stroudsburg, PA: Dowden, Hutchinson & Ross Inc

National Climactic Data Center/National Oceanic and Atmospheric Administration. http://www.ncdc.noaa.gov/climate-information/extreme-events/us-tornado-climatology/tornado-alley (Accessed 02/23/2015)

Nott, J., 2004, Palaeotempestology: the study of prehistoric tropical cyclones - a review and implications for hazard assessment. Environment International 30, 433-447.

National Oceanic and Atmospheric Administration/National Weather Service. 2014a http://www.spc.noaa.gov/wcm/index.html#data. (Accessed 01/03/2014)

National Oceanic and Atmospheric Administration/National Weather Service. 2014b. http://www.srh.noaa.gov/oun/?n=events-20110524-tornado-a1. (Accessed 01/03/2014)

National Oceanic and Atmospheric Administration/Storm Prediction Center. 2015. http://www.spc.noaa.gov/faq/tornado/ef-scale.html. (Accessed 03/20/2015)

Olsen, C.R., Cutshall, N.H., Larsen, I.L., 1982. Pollutant- particle associations and dynamics in coastal marine environments: a review. Marine Chemistry 11, 501-533.

O'Hare, G., 1990, Global warming and extreme weather: a cautionary note. Geography 84, 87-91.

Pearce, F., 1995, Fiddling while Earth warms. New Scientist. 145, 14-15.

Peterson, C.J., 2000, Catastrophic wind damage to North American forests and the potential impact of climate change. The Science of the Total Environment 262, 287-311.

Price, C. and Rind, D., 1992. The effect of climate change on global lightning frequencies, in Proceedings, 9th International Conference on Atmospheric Electricity. Volume 111, St. Petersburg, Russia, 869-872.

Sadeghipour, J., and McClain, T., 1987. Analysis of surface and climactic data for Cheyenne Bottoms. Kansas Geological Survey, Open-file Rept., no. 87-5.

Stanners, D.A., Aston, S.R., 1981. 134Cs:137Cs and 106Ru:137Cs ratios in intertidal sediments from
the Cumbria and Lancashire coasts, England. Estuarine, Coastal and Shelf Science 13, 409-417.

Trapp, R. J., et al. 2007a, Changes in severe thunderstorm environment frequency during the 21st century caused by anthropogenically enhanced global radiative forcing, Proc. Natl. Acad. Sci. U. S. A., 104, 19,719–19,723.

Walker, M., 2005. Quaternary Dating Methods: John Wiley & Sons, Ltd, San Francisco, 304 p.

Wentworth, C.K. 1922. A scale of grade and class terms for clastic sediments. Journal of Geology, 30,
377–392.

Wigley, T. M. L., 1988. The effect of changing climate on the frequency of absolute extreme events, Climate Monitor 17(2), 44-54.

White, R. and D. Etkin. 1997. Climate Change, Extreme Events and the Canadian Insurance Industry. Natural Hazards, 16(2-3): 135-163.

Zimmerman, J.L. 1990. Cheyenne Bottoms: Wetland in jeopardy. University Press of Kansas, Lawrence, Kansas, 197 p.

APPENDICES

A. Cheyenne Bottoms Sediment Data

Mid-point depth in core	% Sand	%Sand Difference	% Sand Difference S.D.	Mean Grain Size	MGS Difference	MGS Difference S.D.
(mm)				ø	ø	ø
1.7	11.7	0.8	0.8	5.6	0.0	0.1
5.1	12.6	-0.6	0.8	5.6	0.0	0.1
8.6	11.9	1.1	0.8	5.6	0.0	0.1
12.0	13.3	-1.0	0.8	5.5	0.0	0.1
15.4	11.7	-0.2	0.8	5.6	0.0	0.1
18.8	11.7	0.5	0.8	5.6	0.0	0.1
22.3	12.4	-0.8	0.8	5.6	0.0	0.1
25.7	11.6	-3.3	0.8	5.6	0.2	0.1
29.1	7.9	2.4	0.8	5.9	-0.2	0.1
32.6	10.4	1.5	0.8	5.6	0.0	0.1
36.0	12.6	-1.5	0.8	5.5	0.1	0.1
39.4	10.9	0.7	0.8	5.6	0.0	0.1
42.8	11.5	-0.6	0.8	5.6	0.0	0.1
46.3	10.8	0.0	0.8	5.6	0.0	0.1
49.7	10.8	-0.5	0.8	5.6	0.0	0.1
53.1	9.1	-0.2	0.8	5.7	-0.1	0.1
56.5	10.4	-1.5	0.8	5.5	0.1	0.1
60.0	8.9	-1.2	0.8	5.7	0.1	0.1
63.4	7.3	-0.4	0.8	5.8	0.0	0.1
66.8	6.8	0.4	0.8	5.9	0.0	0.1
70.2	7.7	-3.1	0.8	5.8	0.4	0.1
73.7	4.5	-0.5	0.8	6.2	0.0	0.1
77.1	4.0	0.2	0.8	6.3	0.1	0.1
80.5	4.1	-0.4	0.8	6.3	-0.2	0.1
83.9	3.2	0.5	0.8	6.2	-0.3	0.1
87.4	3.7	3.4	0.8	5.9	-0.3	0.1
90.8	7.6	-0.1	0.8	5.6	-0.1	0.1
94.2	7.3	3.9	0.8	5.6	-0.2	0.1

Mid-point depth in core	% Sand	%Sand Difference	% Sand Difference S.D.	Mean Grain Size	MGS Difference	MGS Difference S.D.
(mm)				ø	ø	ø
97.7	11.3	0.1	0.8	5.4	0.0	0.1
101.1	12.1	-1.2	0.8	5.4	0.0	0.1
104.5	10.3	0.0	0.8	5.4	0.0	0.1
107.9	10.2	0.4	0.8	5.4	-0.1	0.1
111.4	10.7	0.0	0.8	5.3	0.0	0.1
114.8	10.5	-0.3	0.8	5.3	0.0	0.1
118.2	10.6	-0.2	0.8	5.3	0.0	0.1
121.6	10.2	0.9	0.8	5.3	0.0	0.1
125.1	11.2	0.2	0.8	5.2	0.0	0.1
128.5	11.2	-0.2	0.8	5.3	0.0	0.1
131.9	10.9	-0.4	0.8	5.3	0.0	0.1
135.3	11.1	-0.3	0.8	5.3	0.0	0.1
138.8	10.5	-1.4	0.8	5.3	0.1	0.1
142.2	8.8	1.4	0.8	5.4	0.0	0.1
145.6	10.4	-0.8	0.8	5.4	0.1	0.1
149.0	9.8	-0.7	0.8	5.4	0.0	0.1
152.5	8.7	1.0	0.8	5.5	0.0	0.1
155.9	9.6	0.6	0.8	5.5	0.0	0.1
159.3	10.7	-1.7	0.8	5.4	0.1	0.1
162.7	8.8	-1.6	0.8	5.5	0.1	0.1
166.2	7.2	-0.8	0.8	5.6	0.1	0.1
169.6	6.5	-1.0	0.8	5.7	0.0	0.1
173.0	5.3	-0.3	0.8	5.7	0.0	0.1
176.5	5.1	0.1	0.8	5.7	0.0	0.1
179.9	5.4	-1.5	0.8	5.6	0.1	0.1
183.3	3.9	-0.1	0.8	5.7	0.0	0.1
186.7	3.9	0.9	0.8	5.8	0.0	0.1
190.2	4.9	-0.6	0.8	5.8	0.0	0.1
193.6	4.1	0.5	0.8	5.8	-0.1	0.1
197.0	4.6	0.0	0.8	5.7	0.0	0.1
200.4	4.4	-0.5	0.8	5.7	0.0	0.1
203.9	3.6	1.0	0.8	5.8	-0.1	0.1
207.3	4.7	1.3	0.8	5.7	-0.1	0.1
210.7	6.3	-2.0	0.8	5.6	0.3	0.1
214.1	4.2	-0.8	0.8	5.8	0.2	0.1
217.6	3.4	-1.2	0.8	6.0	0.3	0.1
221.0	2.3	0.0	0.8	6.2	0.0	0.1
224.4	2.2	0.2	0.8	6.2	0.1	0.1
227.8	2.5	-0.3	0.8	6.3	0.2	0.1

Mid-point depth in core	% Sand	%Sand Difference	% Sand Difference S.D.	Mean Grain Size	MGS Difference	MGS Difference S.D.
(mm)				ø	ø	ø
231.3	2.2	0.0	0.8	6.5	0.1	0.1
234.7	2.0	0.7	0.8	6.6	-0.1	0.1
238.1	2.8	-0.2	0.8	6.5	0.0	0.1
241.6	2.5	0.2	0.8	6.5	-0.2	0.1
245.0	2.9	0.2	0.8	6.3	-0.1	0.1
248.4	3.0	-0.1	0.8	6.2	0.0	0.1
251.8	2.9	0.4	0.8	6.1	-0.1	0.1
255.3	3.1	0.7	0.8	6.1	-0.1	0.1
258.7	3.9	0.2	0.8	5.9	0.1	0.1
263.3	4.5	-1.3	0.8	6.0	0.2	0.1
269.0	2.9	-0.6	0.8	6.2	0.1	0.1
274.7	2.1	-0.3	0.8	6.3	0.1	0.1
280.4	2.0	0.5	0.8	6.4	-0.1	0.1
286.1	2.4	0.7	0.8	6.3	-0.3	0.1
291.8	3.1	1.2	0.8	6.0	-0.2	0.1
297.5	4.5	0.0	0.8	5.8	0.0	0.1
303.2	4.4	-0.3	0.8	5.8	0.0	0.1
308.9	4.1	-0.9	0.8	5.8	0.1	0.1
314.6	3.3	0.2	0.8	5.9	0.0	0.1
320.4	3.4	-0.7	0.8	5.9	0.0	0.1
326.1	2.6	0.2	0.8	6.0	0.0	0.1
331.8	3.0	-0.2	0.8	5.9	0.0	0.1
337.5	2.7	0.0	0.8	6.0	0.0	0.1
343.2	2.6	0.1	0.8	6.0	-0.1	0.1
348.9	2.7	0.3	0.8	5.9	0.0	0.1
354.6	3.1	0.7	0.8	5.9	-0.1	0.1
360.3	3.9	0.0	0.8	5.8	0.0	0.1
366.0	4.2	0.0	0.8	5.7	0.1	0.1
371.8	3.8	-0.6	0.8	5.8	0.1	0.1
385.5	3.2	0.4	0.8	5.9	0.0	0.1
391.2	3.6	-0.6	0.8	5.9	0.1	0.1
396.9	2.9	-0.3	0.8	6.0	0.0	0.1
402.6	2.7	0.3	0.8	6.1	0.0	0.1
408.3	3.1	-0.1	0.8	6.0	0.0	0.1
414.0	2.9	-0.4	0.8	6.0	0.0	0.1
419.7	2.5	0.1	0.8	6.1	0.0	0.1
425.4	2.6	0.3	0.8	6.1	0.0	0.1
431.1	3.0	-0.8	0.8	6.0	0.1	0.1
436.9	2.3	0.1	0.8	6.1	-0.1	0.1

Mid-point depth in core	% Sand	%Sand Difference	% Sand Difference S.D.	Mean Grain Size	MGS Difference	MGS Difference S.D.
(mm)				ø	ø	ø
442.6	2.2	-0.3	0.8	6.0	0.1	0.1
448.3	2.3	0.1	0.8	6.1	-0.1	0.1
454.0	2.0	0.7	0.8	6.0	-0.1	0.1
459.7	2.7	-0.1	0.8	6.0	0.0	0.1
465.4	2.4	-0.5	0.8	6.0	0.0	0.1
471.1	2.0	0.7	0.8	6.0	-0.1	0.1
476.8	2.9	0.2	0.8	5.9	0.0	0.1
482.5	2.9	-0.4	0.8	5.9	0.1	0.1
488.2	2.8	-0.5	0.8	6.0	0.1	0.1
494.0	2.4	-0.4	0.8	6.0	0.0	0.1
499.7	1.7	0.2	0.8	6.1	0.0	0.1
505.4	2.0	-0.4	0.8	6.0	0.0	0.1
511.1	1.4	0.7	0.8	6.1	-0.1	0.1
516.8	2.1	-0.8	0.8	6.0	0.1	0.1
522.5	1.4	-0.2	0.8	6.1	0.0	0.1
528.2	1.1	1.0	0.8	6.1	-0.1	0.1
533.9	2.1	0.1	0.8	6.0	0.0	0.1
539.6	2.2	0.2	0.8	6.0	0.0	0.1
545.4	2.4	0.0	0.8	5.9	0.0	0.1
551.1	2.4	0.2	0.8	5.9	0.0	0.1
556.8	2.7	-0.1	0.8	5.9	0.0	0.1
562.5	2.6	-0.5	0.8	5.9	0.0	0.1
568.2	2.0	-0.3	0.8	6.0	0.0	0.1
573.9	1.8	-0.5	0.8	6.0	0.1	0.1
579.6	1.2	-0.8	0.8	6.1	0.0	0.1
585.3	0.5	-0.2	0.8	6.1	0.1	0.1
591.0	0.3	0.1	0.8	6.2	-0.1	0.1
596.7	0.4	0.0	0.8	6.1	0.0	0.1
602.5	0.4	0.0	0.8	6.1	0.0	0.1
608.2	0.4	0.0	0.8	6.1	0.0	0.1
613.9	0.4	0.0	0.8	6.2	0.0	0.1
619.6	0.4	-0.1	0.8	6.2	0.0	0.1
625.3	0.3	0.0	0.8	6.2	0.0	0.1
631.0	0.4	0.0	0.8	6.2	0.0	0.1
636.7	0.4	0.0	0.8	6.2	0.0	0.1
642.4	0.4	0.0	0.8	6.2	0.0	0.1
648.1	0.4	0.1	0.8	6.2	-0.1	0.1
653.9	0.5	0.7	0.8	6.1	0.0	0.1
659.6	1.2	0.1	0.8	6.1	0.0	0.1

Mid-point depth in core	% Sand	%Sand Difference	% Sand Difference S.D.	Mean Grain Size	MGS Difference	MGS Difference S.D.
(mm)				ø	ø	ø
665.3	1.3	-0.5	0.8	6.1	0.0	0.1
671.0	1.1	-0.3	0.8	6.1	0.1	0.1
676.7	0.5	0.0	0.8	6.2	0.0	0.1
682.4	0.5	0.0	0.8	6.2	0.0	0.1
688.1	0.5	0.0	0.8	6.1	0.0	0.1
693.8	0.4	0.0	0.8	6.2	0.1	0.1
699.5	0.4	0.1	0.8	6.3	0.0	0.1
705.2	0.4	0.1	0.8	6.3	0.1	0.1
711.0	0.8	-0.2	0.8	6.3	0.1	0.1
716.7	0.3	0.1	0.8	6.4	-0.1	0.1
722.4	0.4	0.0	0.8	6.4	-0.1	0.1
728.1	0.4	0.0	0.8	6.2	0.0	0.1
733.8	0.5	1.0	0.8	6.2	-0.1	0.1
739.5	1.5	0.4	0.8	6.0	-0.1	0.1
745.2	1.9	-1.1	0.8	5.9	0.1	0.1
750.9	0.5	0.6	0.8	6.1	-0.1	0.1
756.6	1.4	-0.9	0.8	6.0	0.1	0.1
762.4	0.5	0.7	0.8	6.1	0.1	0.1
768.1	1.2	-0.7	0.8	6.2	0.0	0.1
773.8	0.4	0.0	0.8	6.2	0.1	0.1
779.5	0.5	0.2	0.8	6.3	0.0	0.1
785.2	0.5	-0.4	0.8	6.3	0.2	0.1
790.9	0.2	0.6	0.8	6.5	-0.1	0.1
796.6	1.2	-0.4	0.8	6.3	0.1	0.1
802.3	0.5	0.0	0.8	6.4	0.1	0.1
808.0	0.4	0.0	0.8	6.5	0.0	0.1
813.7	0.4	0.0	0.8	6.5	0.0	0.1
819.5	0.4	-0.1	0.8	6.5	0.0	0.1
825.2	0.3	0.1	0.8	6.5	-0.1	0.1
830.9	0.4	-0.1	0.8	6.5	0.1	0.1
836.6	0.4	0.0	0.8	6.5	0.0	0.1
842.3	0.4	-0.1	0.8	6.5	0.1	0.1
848.0	0.4	0.1	0.8	6.6	-0.1	0.1
853.7	0.3	0.0	0.8	6.5	0.0	0.1
859.4	0.3	-0.1	0.8	6.6	0.0	0.1
865.1	0.3	0.1	0.8	6.6	-0.1	0.1
870.9	0.4	0.0	0.8	6.5	0.0	0.1
876.6	0.4	-0.1	0.8	6.5	-0.2	0.1
882.3	0.3	0.2	0.8	6.3	-0.1	0.1

Mid-point depth in core	% Sand	%Sand Difference	% Sand Difference S.D.	Mean Grain Size	MGS Difference	MGS Difference S.D.
(mm)				ø	ø	ø
888.0	0.5	-0.1	0.8	6.2	0.3	0.1
893.7	0.4	-0.4	0.8	6.5	0.3	0.1
899.4	0.0	0.4	0.8	6.8	-0.3	0.1
905.1	0.4	-0.1	0.8	6.5	0.0	0.1
910.8	0.4	-0.1	0.8	6.5	0.1	0.1
916.5	0.3	0.1	0.8	6.6	-0.1	0.1
922.2	0.4	0.0	0.8	6.5	0.0	0.1
928.0	0.4	0.0	0.8	6.5	0.0	0.1
933.7	0.4	0.0	0.8	6.5	0.0	0.1
939.4	0.3	0.1	0.8	6.6	-0.1	0.1
945.1	0.4	0.0	0.8	6.5	0.0	0.1
950.8	0.4	0.0	0.8	6.5	0.0	0.1
956.5	0.4	0.0	0.8	6.5	0.0	0.1
962.2	0.4	0.0	0.8	6.5	0.0	0.1
967.9	0.4	0.0	0.8	6.5	-0.1	0.1
973.6	0.4	0.0	0.8	6.4	0.0	0.1
979.4	0.4	-0.1	0.8	6.4	0.0	0.1
985.1	0.2	0.1	0.8	6.5	0.0	0.1
990.8	0.3	0.2	0.8	6.4	-0.2	0.1
996.5	0.5	0.0	0.8	6.3	0.0	0.1
1002.2	0.4	-0.2	0.8	6.3	0.1	0.1
1007.9	0.3	0.1	0.8	6.4	-0.1	0.1
1013.6	0.4	-0.4	0.8	6.3	-0.2	0.1
1025.0	2.3	-2.3	0.8	6.1	0.5	0.1
1036.5	0.0	0.0	0.8	6.6	0.0	0.1
1042.2	0.0	0.0	0.8	6.6		0.1

B. Canton Lake Sediment Data

Mid-point depth in core	% Sand	% Sand Difference	% Sand Difference S.D.	Mean Grain Size	MGS Difference	MGS Difference S.D.
(mm)				Ø	Ø	Ø
1.6	0.1	-0.1	6.0	6.3	0.1	0.2
4.8	0.0	0.2	6.0	6.3	-0.1	0.2
8.0	0.2	-0.1	6.0	6.3	0.0	0.2
11.2	0.1	1.5	6.0	6.3	-0.1	0.2
15.4	1.7	0.4	6.0	6.2	0.0	0.2
19.7	2.1	7.0	6.0	6.1	-0.3	0.2
22.9	9.1	-3.2	6.0	5.9	0.1	0.2
27.1	5.8	4.7	6.0	6.0	-0.2	0.2
32.4	10.5	1.6	6.0	5.8	-0.1	0.2
36.7	12.1	-2.1	6.0	5.7	0.1	0.2
39.9	10.0	-2.9	6.0	5.8	0.1	0.2
44.1	7.1	1.4	6.0	5.9	-0.1	0.2
49.5	8.5	25.1	6.0	5.8	-1.1	0.2
54.8	33.5	-18.1	6.0	4.6	0.8	0.2
59.0	15.5	-2.9	6.0	5.5	0.1	0.2
62.2	12.5	-4.6	6.0	5.6	0.2	0.2
65.4	7.9	6.6	6.0	5.7	-0.2	0.2
68.6	14.6	6.2	6.0	5.5	-0.2	0.2
71.8	20.8	-0.4	6.0	5.3	0.0	0.2
75.0	20.4	2.3	6.0	5.3	-0.1	0.2
78.2	22.7	-6.9	6.0	5.2	0.3	0.2
81.4	15.9	14.0	6.0	5.5	-0.5	0.2
84.6	29.9	3.1	6.0	5.0	-0.2	0.2
87.8	32.9	5.9	6.0	4.9	-0.2	0.2
92.0	38.9	0.6	6.0	4.6	0.0	0.2
96.3	39.5	-2.6	6.0	4.6	0.1	0.2
99.5	36.8	3.1	6.0	4.7	-0.1	0.2
102.7	39.9	-10.7	6.0	4.5	0.3	0.2
106.9	29.3	9.5	6.0	4.9	-0.3	0.2
112.2	38.7	-6.2	6.0	4.6	0.2	0.2
116.5	32.5	8.7	6.0	4.8	-0.3	0.2
119.7	41.2	7.2	6.0	4.5	-0.2	0.2
122.9	48.4	-0.9	6.0	4.3	0.0	0.2

Mid-point depth in core	% Sand	% Sand Difference	% Sand Difference S.D.	Mean Grain Size	MGS Difference	MGS Difference S.D.
(mm)				Ø	Ø	Ø
126.1	47.5	1.7	6.0	4.3	-0.1	0.2
129.3	49.2	-1.2	6.0	4.2	0.1	0.2
132.4	48.0	2.2	6.0	4.4	-0.1	0.2
135.6	50.1	-1.9	6.0	4.2	0.1	0.2
138.8	48.2	-3.5	6.0	4.3	0.1	0.2
142.0	44.8	0.3	6.0	4.4	0.0	0.2
145.2	45.0	3.3	6.0	4.4	-0.1	0.2
148.4	48.4	-2.9	6.0	4.3	0.1	0.2
152.7	45.5	-2.0	6.0	4.3	0.1	0.2
156.9	43.5	-10.6	6.0	4.4	0.4	0.2
160.1	32.9	6.0	6.0	4.8	-0.2	0.2
163.3	38.8	-2.4	6.0	4.6	0.1	0.2
166.5	36.4	4.9	6.0	4.7	-0.2	0.2
169.7	41.3	-2.7	6.0	4.6	0.1	0.2
172.9	38.6	7.5	6.0	4.7	-0.3	0.2
176.1	46.1	-3.7	6.0	4.4	0.1	0.2
179.3	42.4	2.0	6.0	4.5	-0.1	0.2
183.5	44.4	-5.3	6.0	4.5	0.2	0.2
187.8	39.1	-5.2	6.0	4.7	0.2	0.2
191.0	33.9	0.0	6.0	4.9	0.0	0.2
194.1	34.0	-2.3	6.0	4.9	0.1	0.2
197.3	31.7	7.0	6.0	5.0	-0.2	0.2
200.5	38.7	-2.4	6.0	4.7	0.1	0.2
203.7	36.3	3.6	6.0	4.9	-0.1	0.2
206.9	39.9	-1.6	6.0	4.7	0.0	0.2
211.2	38.3	4.0	6.0	4.7	-0.2	0.2
215.4	42.3	3.8	6.0	4.6	-0.1	0.2
218.6	46.1	8.2	6.0	4.5	-0.2	0.2
221.8	54.3	3.7	6.0	4.3	-0.2	0.2
225.0	58.0	5.2	6.0	4.1	-0.2	0.2
231.9	63.1	1.9	6.0	3.9	-0.1	0.2
239.9	65.0	-1.1	6.0	3.9	0.0	0.2
247.9	63.9	0.8	6.0	3.9	0.0	0.2
258.5	64.7	2.0	6.0	3.9	-0.1	0.2
269.1	66.7	-0.7	6.0	3.8	0.0	0.2
279.8	66.0	4.5	6.0	3.8	-0.1	0.2
286.7	70.5	-4.5	6.0	3.7	0.1	0.2
291.0	66.0	-10.4	6.0	3.8	0.3	0.2
296.3	55.6	0.6	6.0	4.1	0.0	0.2

Mid-point depth in core	% Sand	% Sand Difference	% Sand Difference S.D.	Mean Grain Size	MGS Difference	MGS Difference S.D.
(mm)				Ø	Ø	Ø
300.5	56.2	0.3	6.0	4.1	0.0	0.2
303.7	56.5	-0.8	6.0	4.1	0.0	0.2
306.9	55.7	-4.7	6.0	4.1	0.1	0.2
311.2	50.9	-1.2	6.0	4.2	0.0	0.2
315.4	49.7	1.7	6.0	4.3	-0.1	0.2
318.6	51.4	2.5	6.0	4.2	-0.1	0.2
322.9	53.9	-4.2	6.0	4.1	0.1	0.2
328.2	49.7	1.5	6.0	4.2	-0.1	0.2
333.5	51.2	-6.6	6.0	4.2	0.2	0.2
337.8	44.7	-12.7	6.0	4.4	0.4	0.2
341.0	32.0	17.5	6.0	4.8	-0.6	0.2
345.2	49.5	-1.9	6.0	4.3	0.1	0.2
350.5	47.6	-1.8	6.0	4.3	0.1	0.2
354.8	45.8	-3.9	6.0	4.4	0.1	0.2
359.0	41.9	7.0	6.0	4.5	-0.2	0.2
364.4	48.9	6.0	6.0	4.3	-0.2	0.2
369.7	54.9	8.8	6.0	4.1	-0.2	0.2
377.7	63.7	-1.6	6.0	3.9	0.1	0.2
385.6	62.1	5.0	6.0	3.9	-0.1	0.2
393.6	67.0	0.5	6.0	3.8	0.0	0.2
401.6	67.6	-2.2	6.0	3.8	0.1	0.2
409.6	65.3	5.1	6.0	3.9	-0.2	0.2
417.6	70.4	-2.9	6.0	3.7	0.1	0.2
422.9	67.5	-2.1	6.0	3.8	0.0	0.2
428.2	65.5	-5.7	6.0	3.8	0.1	0.2
433.5	59.7	-12.7	6.0	4.0	0.3	0.2
438.8	47.0	6.4	6.0	4.3	-0.2	0.2
446.8	53.5	7.7	6.0	4.1	-0.2	0.2
454.8	61.1	11.6	6.0	3.9	-0.3	0.2
460.1	72.7	-1.4	6.0	3.6	0.0	0.2
468.1	71.3	-2.5	6.0	3.6	0.1	0.2
478.7	68.8	1.6	6.0	3.7	-0.1	0.2
489.4	70.4	3.0	6.0	3.7	-0.1	0.2
500.0	73.5	-3.4	6.0	3.6	0.1	0.2
508.0	70.0	1.1	6.0	3.7	0.0	0.2
513.3	71.1	-3.5	6.0	3.7	0.1	0.2
521.3	67.7	0.9	6.0	3.8	0.0	0.2
529.3	68.6	3.4	6.0	3.7	-0.1	0.2
534.6	72.0	4.0	6.0	3.7	-0.1	0.2

Mid-point depth in core	% Sand	% Sand Difference	% Sand Difference S.D.	Mean Grain Size	MGS Difference	MGS Difference S.D.
(mm)				Ø	Ø	Ø
539.9	75.9	-2.4	6.0	3.5	0.1	0.2
545.2	73.6	-7.1	6.0	3.6	0.2	0.2
550.5	66.4	2.8	6.0	3.8	-0.1	0.2
555.9	69.2	2.0	6.0	3.7	0.0	0.2
560.1	71.2	-4.4	6.0	3.7	0.1	0.2
564.4	66.8	-1.3	6.0	3.8	0.0	0.2
569.7	65.4	-1.0	6.0	3.8	0.1	0.2
573.9	64.4	1.0	6.0	3.9	0.0	0.2
577.1	65.4	-0.8	6.0	3.8	0.0	0.2
580.3	64.7	1.2	6.0	3.9	0.0	0.2
583.5	65.9	-3.6	6.0	3.8	0.1	0.2
586.7	62.3	2.7	6.0	4.0	-0.1	0.2
589.9	64.9	-3.1	6.0	3.9	0.1	0.2
593.1	61.8	-3.5	6.0	4.0	0.1	0.2
596.3	58.3	5.9	6.0	4.0	-0.1	0.2
599.5	64.2	-6.0	6.0	3.9	0.2	0.2
603.7	58.2	5.2	6.0	4.1	-0.1	0.2
608.0	63.4	-1.1	6.0	3.9	0.0	0.2
612.2	62.3	9.2	6.0	3.9	-0.2	0.2
617.6	71.4	-4.2	6.0	3.7	0.1	0.2
622.9	67.2	-9.4	6.0	3.8	0.3	0.2
628.2	57.8	3.0	6.0	4.1	-0.1	0.2
633.5	60.8	-4.0	6.0	4.1	0.1	0.2
637.8	56.8	-9.6	6.0	4.1	0.2	0.2
641.0	47.2	-17.2	6.0	4.4	0.4	0.2
645.2	30.0	-1.1	6.0	4.8	0.0	0.2
649.5	28.9	5.5	6.0	4.8	-0.2	0.2
653.7	34.4	16.4	6.0	4.6	-0.4	0.2
661.7	50.8	13.1	6.0	4.2	-0.3	0.2
668.6	63.9	-4.2	6.0	3.9	0.1	0.2
672.9	59.8	-9.1	6.0	4.0	0.2	0.2
677.1	50.7	-6.1	6.0	4.2	0.2	0.2
681.4	44.5	2.9	6.0	4.4	-0.1	0.2
685.6	47.5	15.2	6.0	4.3	-0.4	0.2
689.9	62.7	-7.2	6.0	4.0	0.2	0.2
694.1	55.4	7.4	6.0	4.1	-0.1	0.2
697.3	62.8	2.8	6.0	4.0	-0.1	0.2
700.5	65.6	1.4	6.0	3.9	0.0	0.2
703.7	67.0	-3.7	6.0	3.9	0.1	0.2

Mid-point depth in core	% Sand	% Sand Difference	% Sand Difference S.D.	Mean Grain Size	MGS Difference	MGS Difference S.D.
(mm)				Ø	Ø	Ø
708.0	63.3	-7.4	6.0	4.0	0.2	0.2
713.3	55.9	-0.4	6.0	4.2	0.0	0.2
717.6	55.5	-5.1	6.0	4.2	0.1	0.2
720.7	50.3	0.2	6.0	4.3	0.0	0.2
725.0	50.5	-2.8	6.0	4.3	0.1	0.2
730.3	47.6	3.4	6.0	4.4	-0.1	0.2
735.6	51.0	-0.5	6.0	4.3	0.0	0.2
741.0	50.5	0.9	6.0	4.3	0.0	0.2
745.2	51.3	1.1	6.0	4.2	0.0	0.2
748.4	52.4	-52.4	6.0	4.2	-4.2	0.2

VITA

Mark Samson McCollum

Candidate for the Degree of

Master of Science

Thesis: THE GEOLOGIC RECORD OF PALEOSTORMS FROM LAKE AND WETLAND SEDIMENTS OF THE GREAT PLAINS

Major Field: Geology

Biographical:

Education:

Completed the requirements for the Master of Science in geology at Oklahoma State University, Stillwater, Oklahoma in May, 2015

Completed the requirements for the Bachelor of Science in geology at Baylor University, Waco, Texas in May, 2013

Experience:

Harding and Shelton Exploration Geologist – September 2014 to May 2015
Chesapeake Energy Intern Geologist – May 2014 to August 2014
Head Teaching Assistant – August 2014 to May 2015
Teaching Assistant – August 2013 to May 2014

Professional Memberships:

American Association of Petroleum Geologists – August 2010 to Present
Geological Society of America – August 2010 to Present
Society of Exploration Geophysists – August 2010 to Present
Oklahoma City Geological Society – September 2013 – Present
Houston Geological Society – April 2015 - Present
Society for Sedimentary Geologists – April 2014 – Present

Publications:

McCollum, M.S., Donoghue, J.F., Lutiker, Michelle A., Sanders, Hannah, and McNabb, Tyler, 2015, Investigating the geologic record of paleo-storms from lake and wetland sediments of the Great Plains: Geological Society of America *Abstracts with Programs.* Vol. 47, No. 1, p.53